



# 超高エネルギーガンマ線 天体物理学

Very-high-energy Gamma-ray Astrophysics

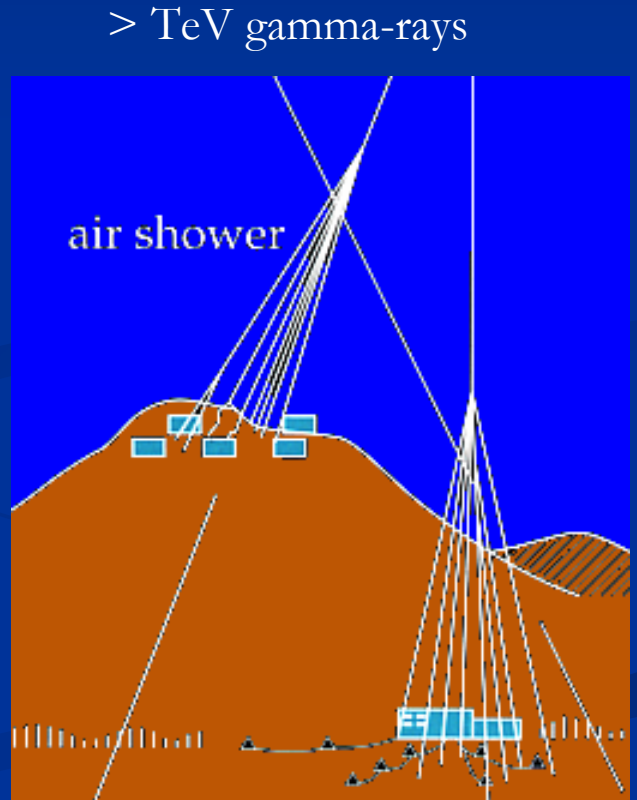
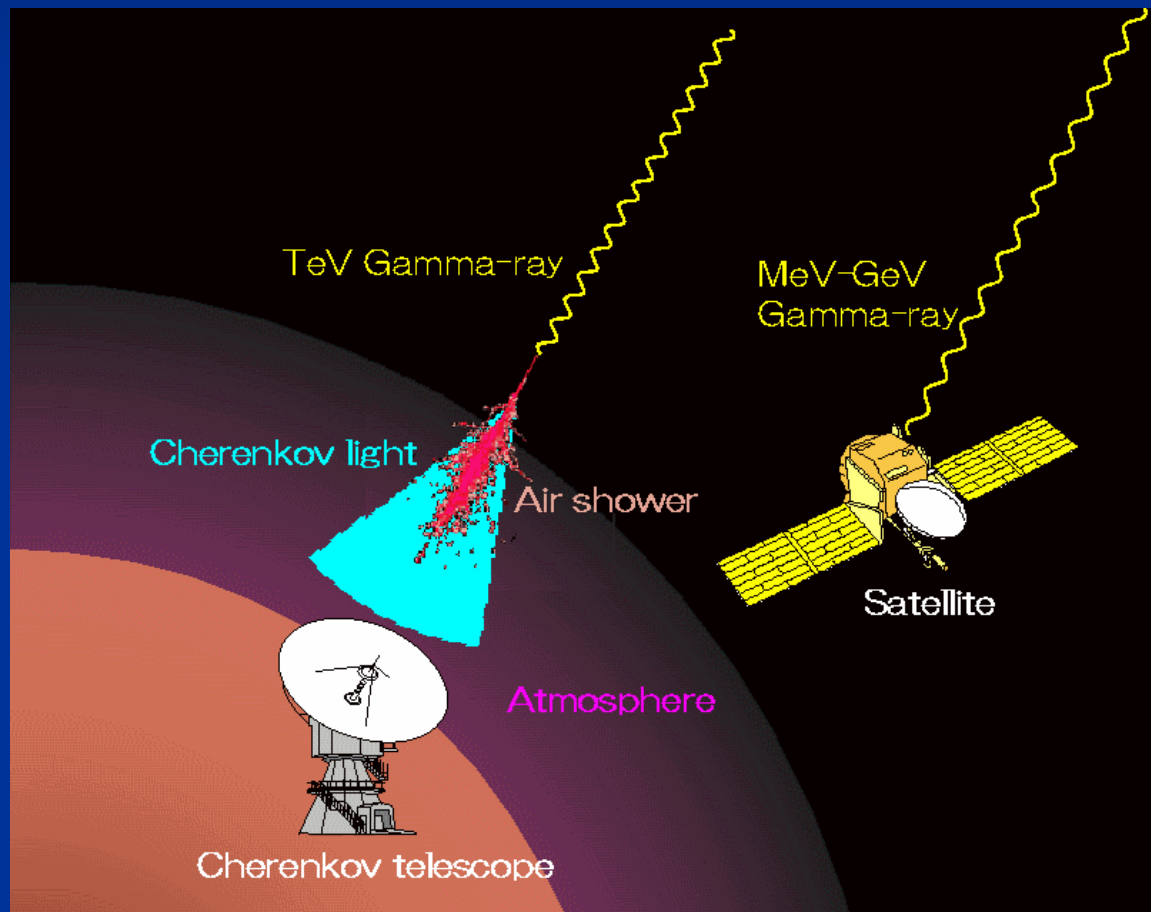
森 正樹  
東京大学宇宙線研究所

第18回理論懇シンポジウム「高エネルギー天体物理学の最前線」

2005年12月25日(日) - 27日(火)

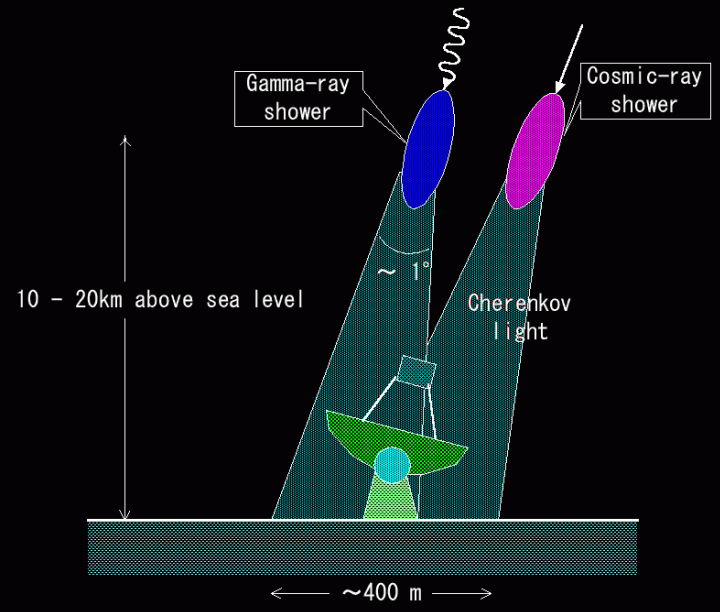
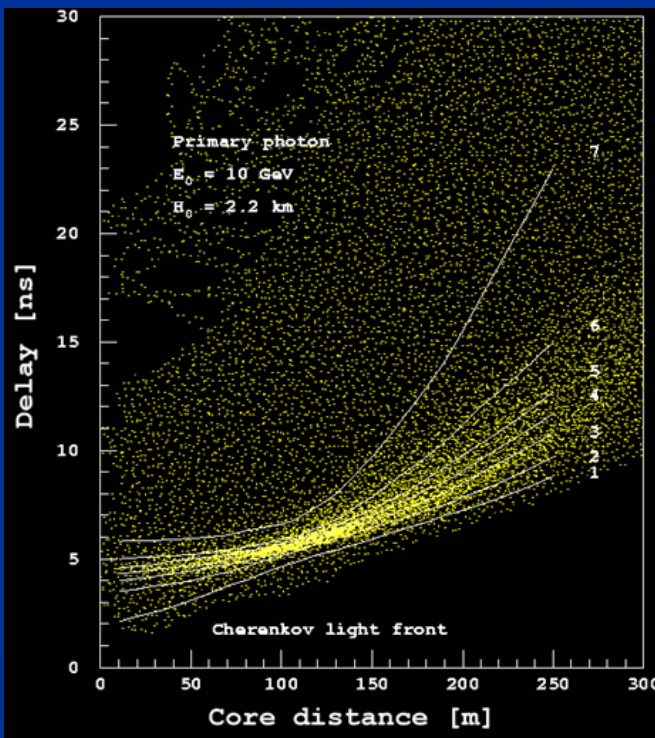
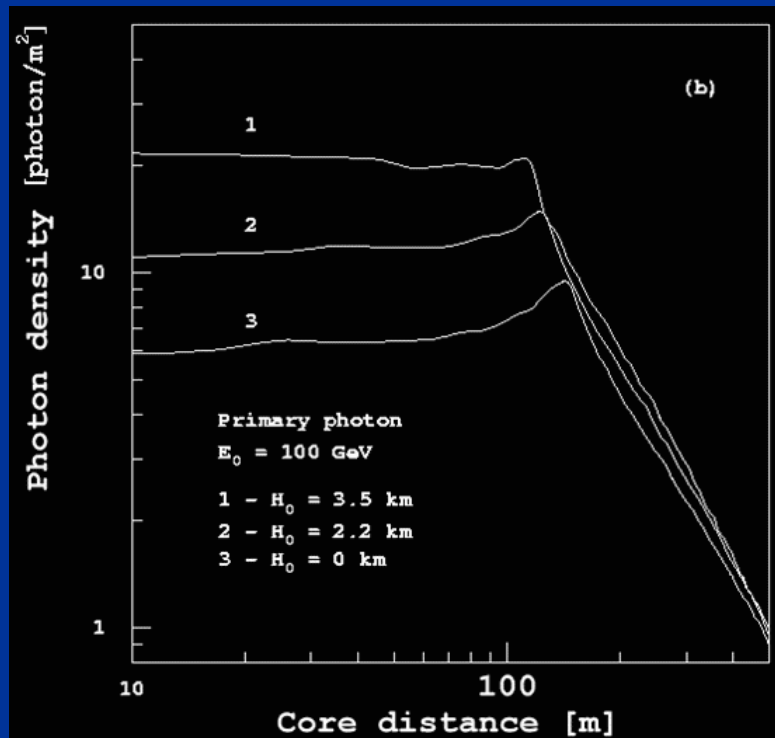
京都大学基礎物理学研究所 湯川記念館 大講演室

# Detection of gamma-rays (1)



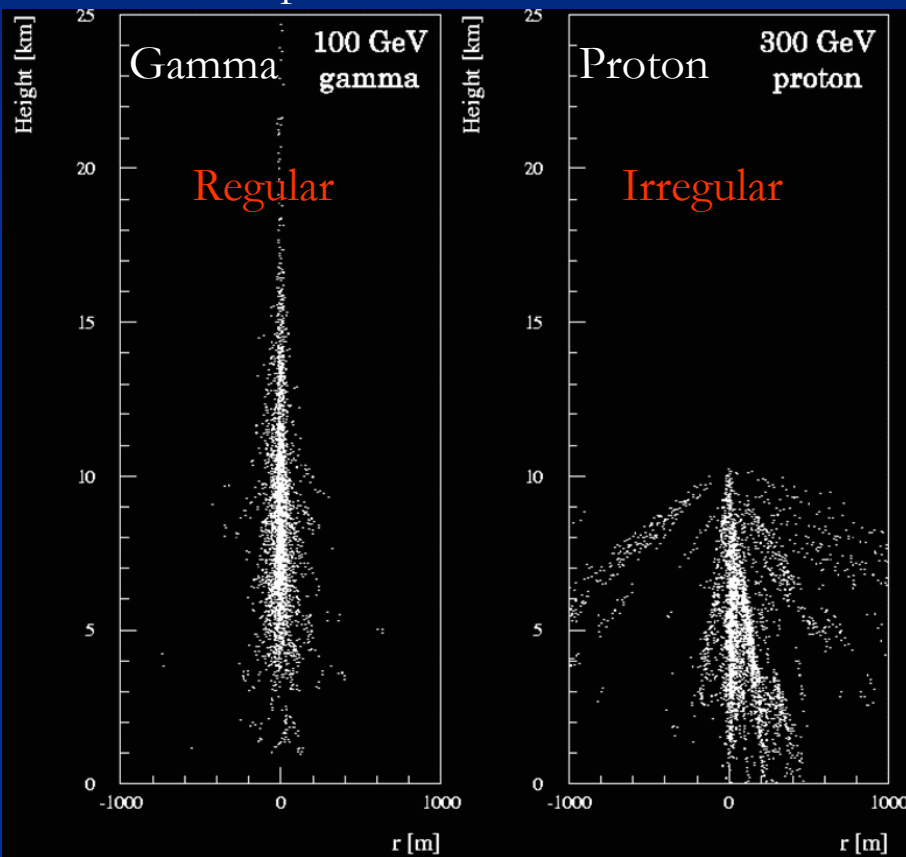
# Atmospheric Cherenkov telescopes

Cherenkov light from gamma-ray showers  
*Lateral distribution*  $\wp$  *Timing distribution*

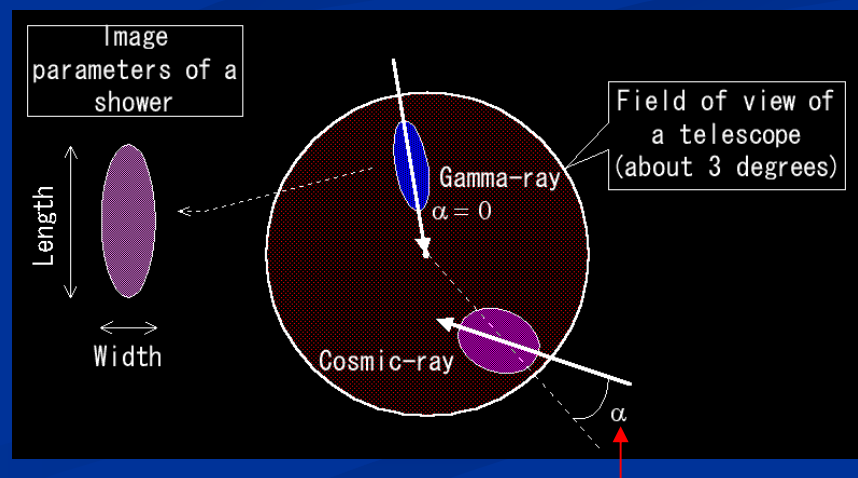
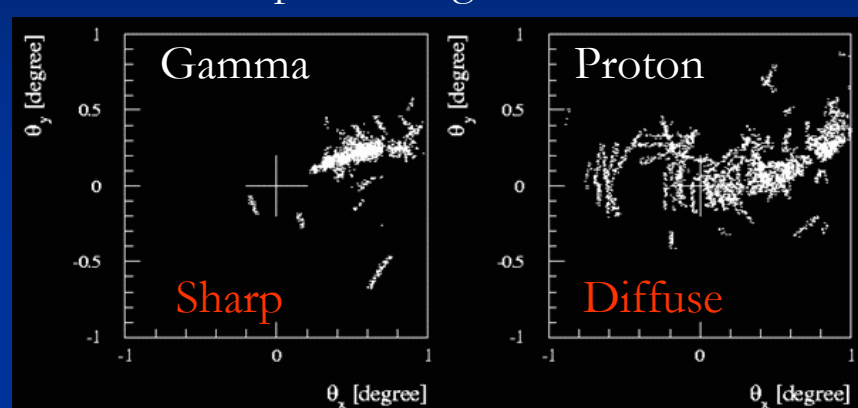


# Imaging Cherenkov Telescopes

Shower profile



Focal plane image



$\alpha$  (image orientation angle)

# Detection of gamma-rays (2)

Base	Satellite	Ground	Ground
Gamma-ray detection	Direct (pair creation)	Indirect (atmospheric Cherenkov)	Indirect (shower array)
Energy	< 30 GeV $\rightarrow$ 100 GeV	>100 GeV $\rightarrow$ 50 GeV	>3 TeV $\rightarrow$ 1 TeV
Pros	High S/N Large FOV	Large area Good $\Delta\theta$	24hr operation Large FOV
Cons	Small area High cost	Low S/N (CR bkgd.) <i>(but imaging overcomes this!)</i> Small FOV	Low S/N (CR bkgd.) Moderate $\Delta\theta$

# VHE Experimental World

MILAGRO



STACEE



MAGIC



TIBET



MILAGRO

STACEE

VERITAS



MAGIC

TACTIC

TIBET  
ARGO-YBJ

PACT

GRAPES

TACTIC



HESS

CANGAROO III

HESS



CANGAROO



# Galactic sources: basics

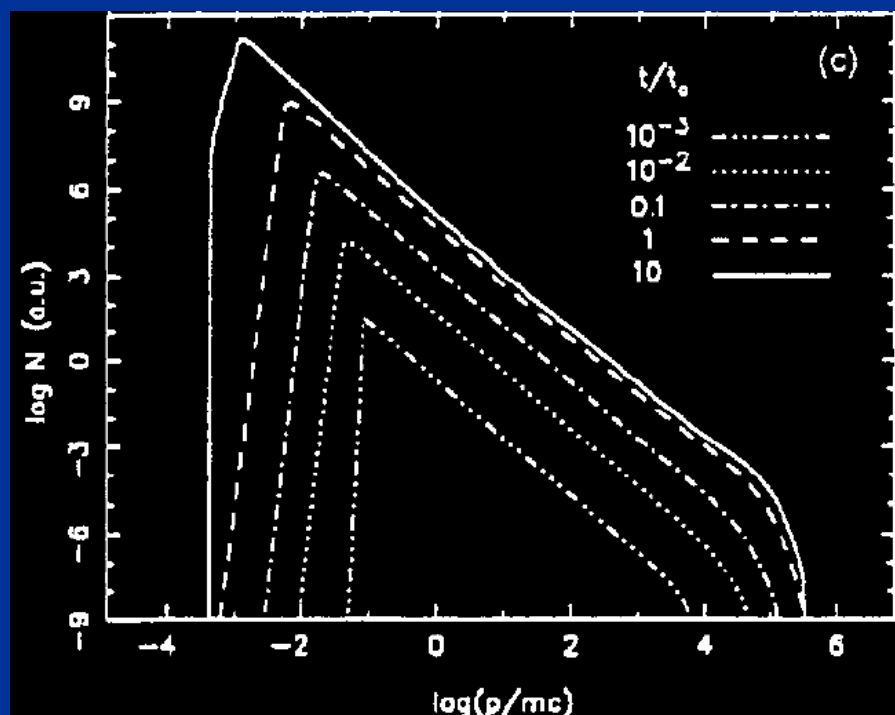
- Supernova remnants = Origin of CR?
  - Energetics – OK (if 10% of  $E_{\text{SN}}$  goes to CR)
  - Maximum energy – Up to “Knee region”
  - How much of them?
  - Some evidences, which can be ascribed to HE electrons:  
where are HE protons?
- Pulsar and pulsar wind nebula (plerions)
  - Crab – “The standard candle”
    - Up to a few 10GeV: pulsed+unpulsed
    - Above: unpulsed only
    - - Unpulsed: SSC (Synchrotron-Self-Compton) model
    - - Where is the cutoff?
    - - (Pulsar emission models)
  - Others? Vela, PSR1706-44,...

# Particle acceleration in SNR

Non-linear kinetic theory

$$t_0 = R_0/v_0; \text{ sweep up time}$$

Particle spectrum



Maximum momentum

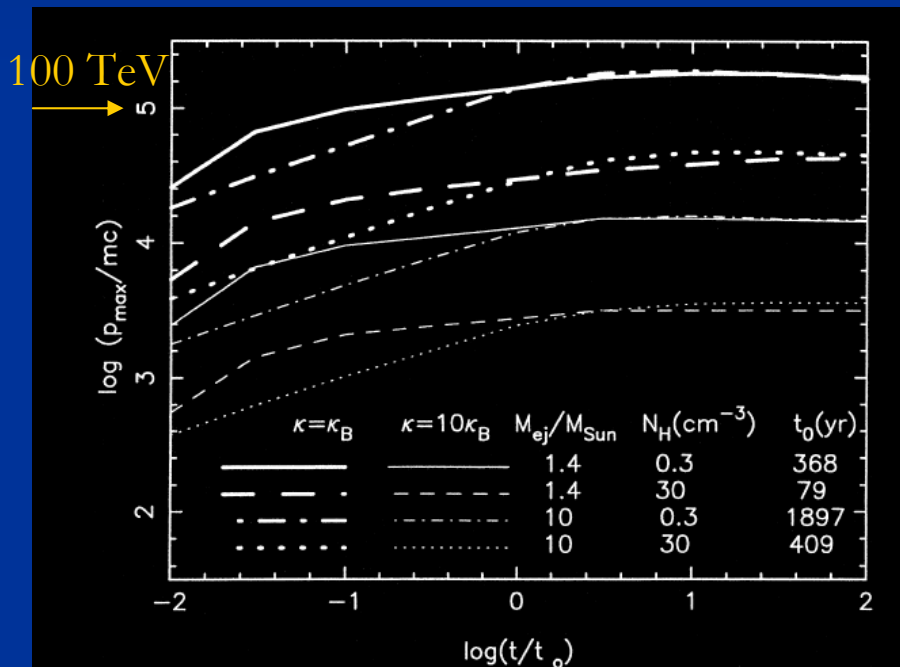


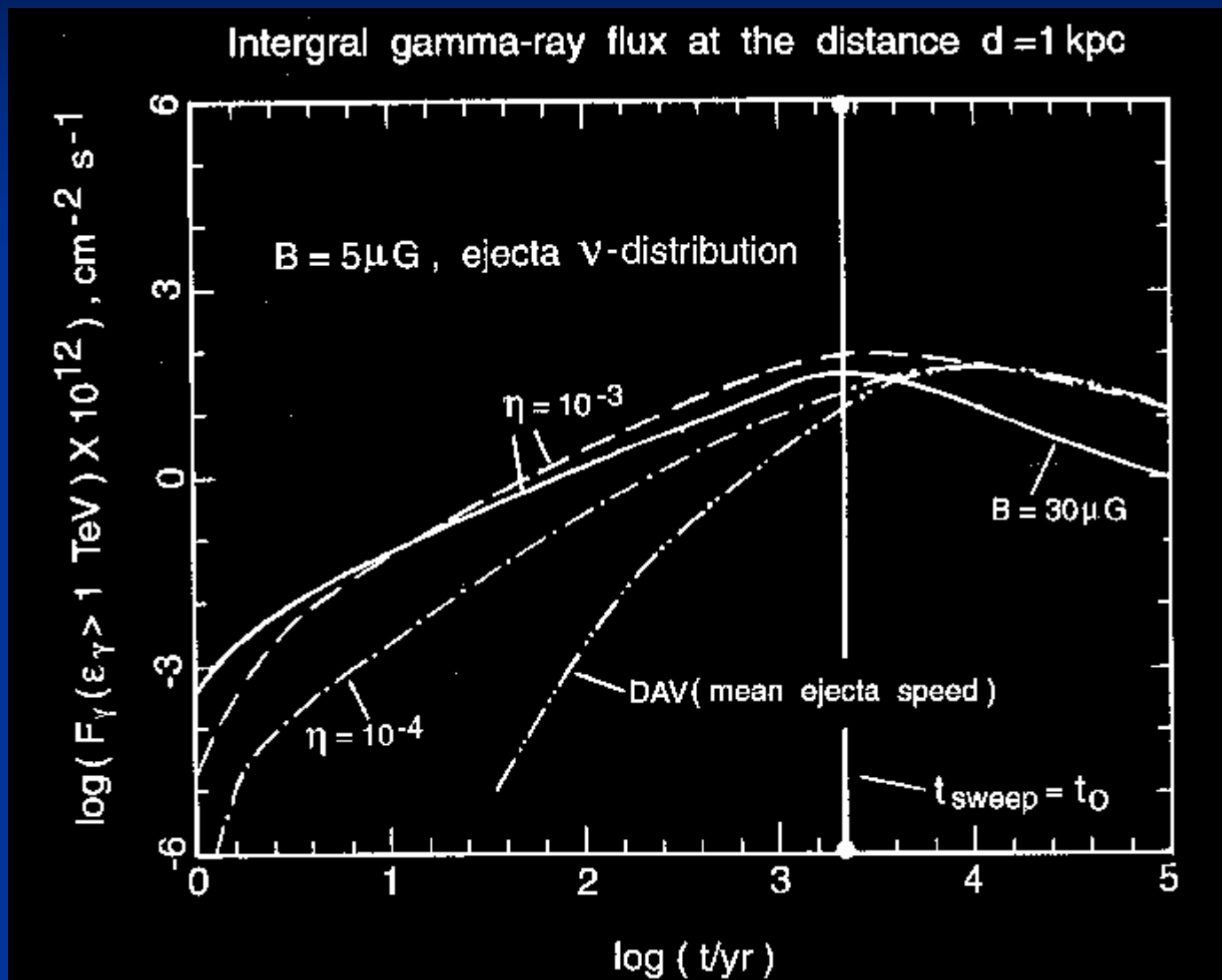
Fig. 2. The maximum CR momentum as a function of time for the same cases as in Fig. 1.

Berezhko & Voelk, APh 1997

Berezhko & Voelk, APh 2000

Cf. Lagage and Cesarsky 1984

# Nuclear gamma-ray flux from SNR

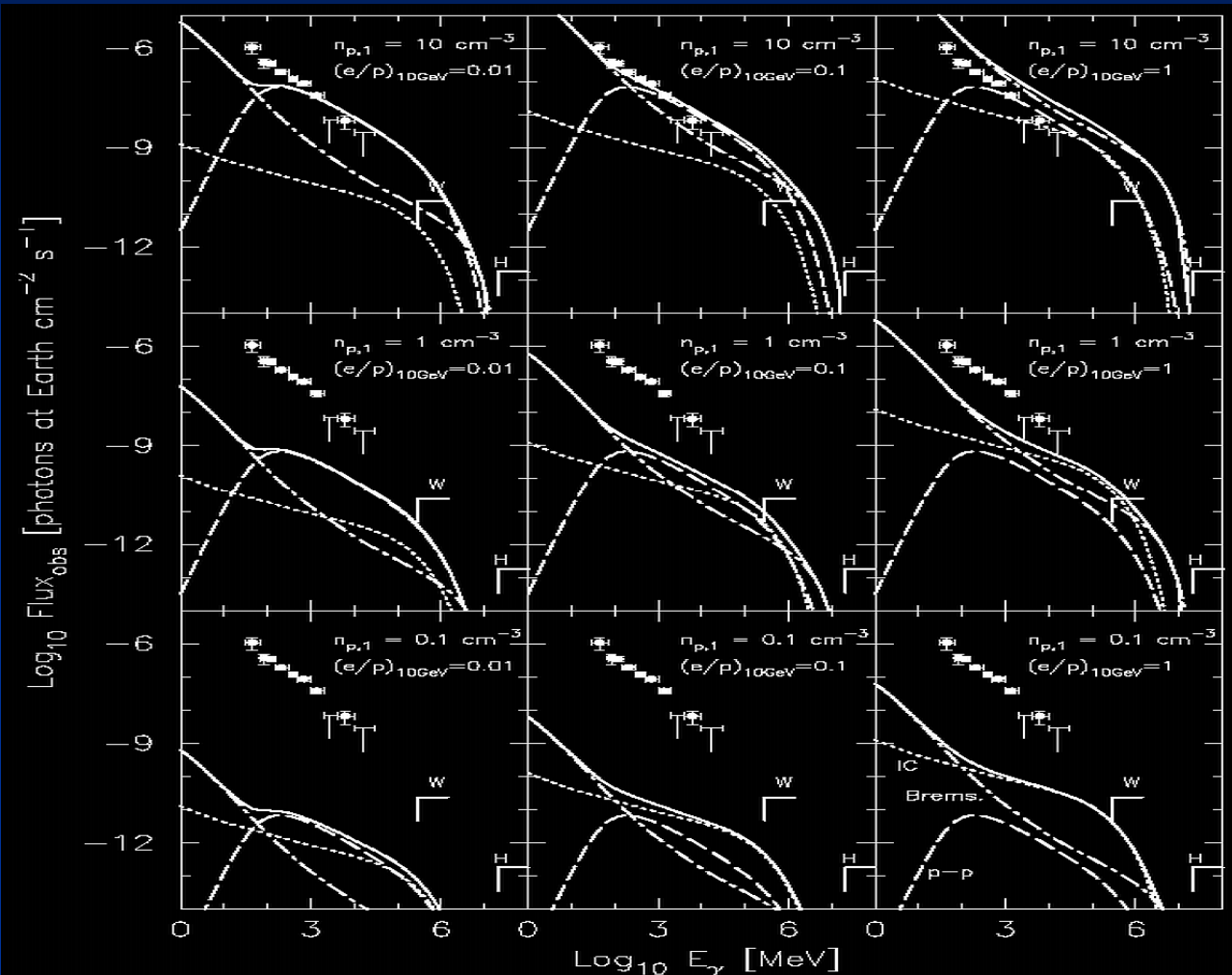


# Gamma-ray emission from SNR

$n = 10 \text{ cm}^{-3}$

$n = 1 \text{ cm}^{-3}$

$n = 0.1 \text{ cm}^{-3}$

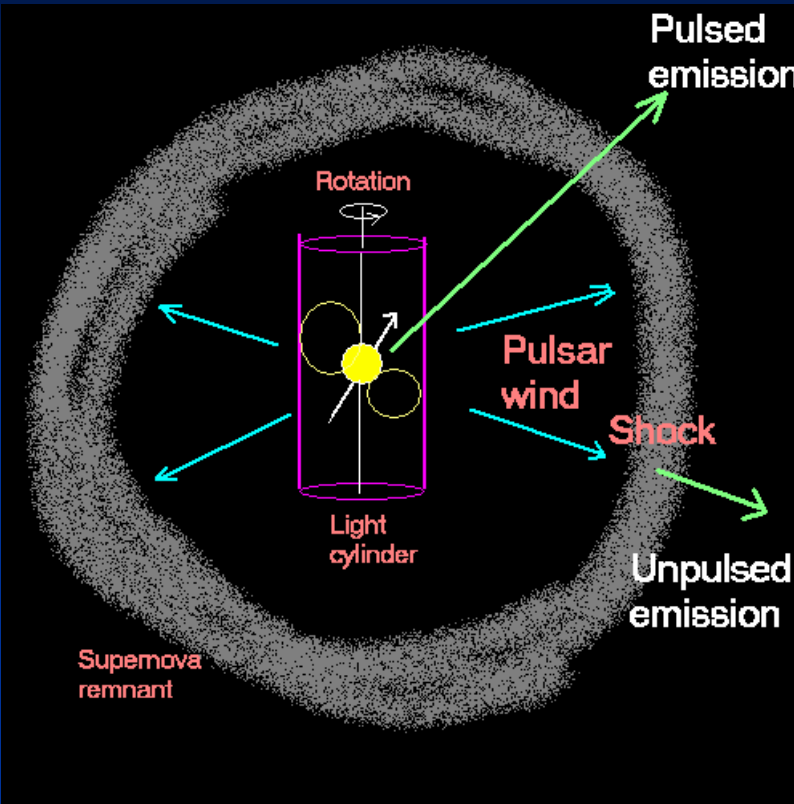


$e/p = 0.01$

$0.1$

$1$

# Pulsar nebula



- A shock is formed when pulsar wind balances with ambient gas pressure, and the wind shines by synchrotron emission by thermalization

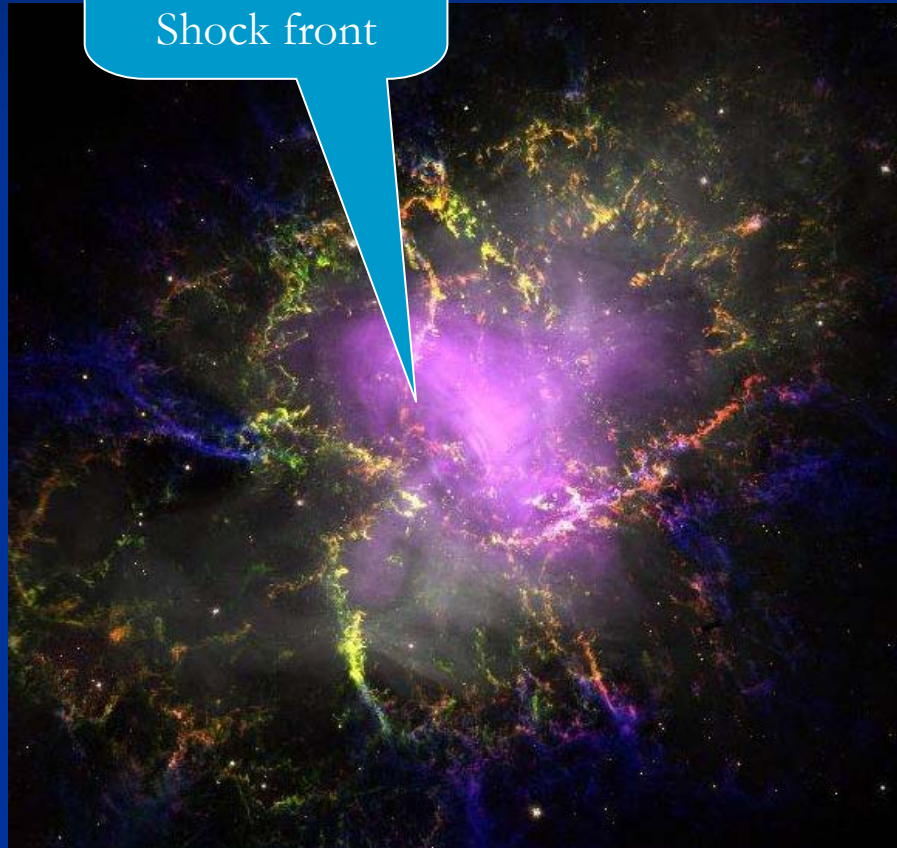


# The Crab

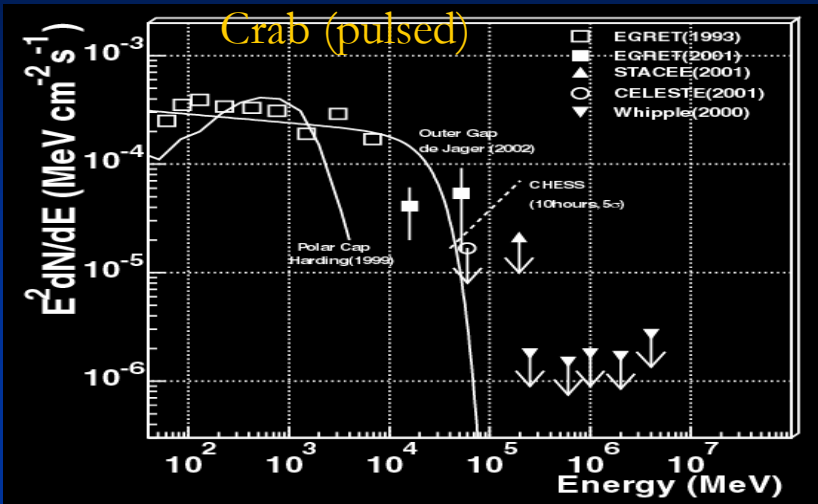
Inner ring

=

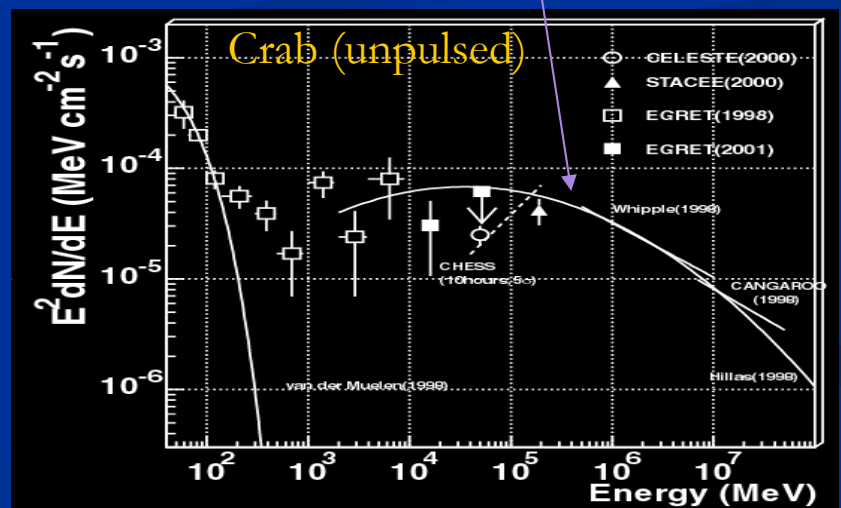
Shock front



Optical + X-ray image



Synchrotron Self Compton



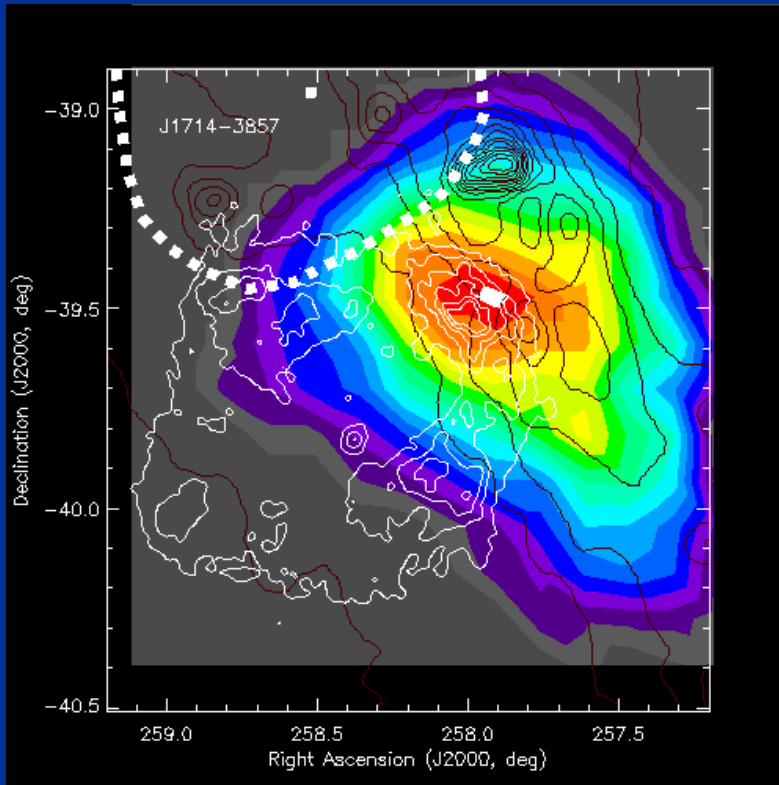
# “Known” galactic sources: Supernova remnants

- **Crab** “The standard candle”
  - Well established (many observations since 1989)
- Supernova remnant **RX J1713.7-3946**
  - CANGAROO 2000/2002, H.E.S.S. 2004
- Supernova remnant **Cas A**
  - HEGRA CT system 2001
- Supernova remnant **RX J0852.0-4622**
  - CANGAROO 2005, H.E.S.S. 2005
- Supernova remnant **G0.9+0.1** [H.E.S.S. 2005]
- Possible SNRs: G338.3-0.0, G8.7-0.1, G18.0-0.7,  
G23.3-0.3, G25.5+0.0, AX J1813-178 [H.E.S.S. 2005]
- Pulsar PSR 1706-44, Vela pulsar, SN1006
  - CANGAROO-I claims, but H.E.S.S. upper limits

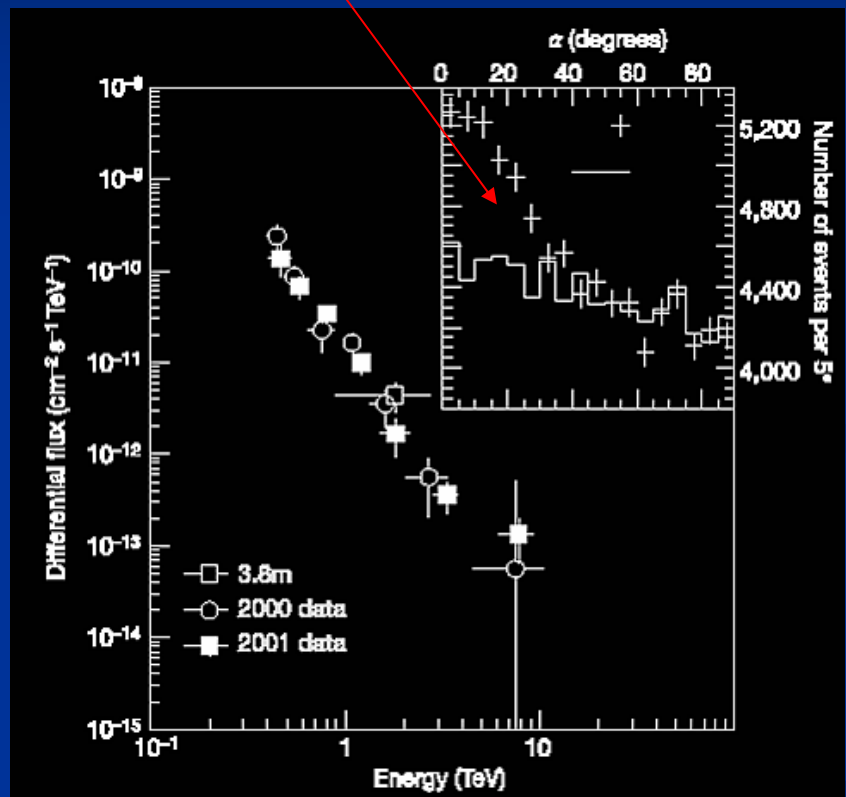
# SNR RX J1713.7-3946 (1)

Gamma-ray signal = (ON) – (OFF)

- Detected in X-rays
- Non-thermal X-ray spectrum

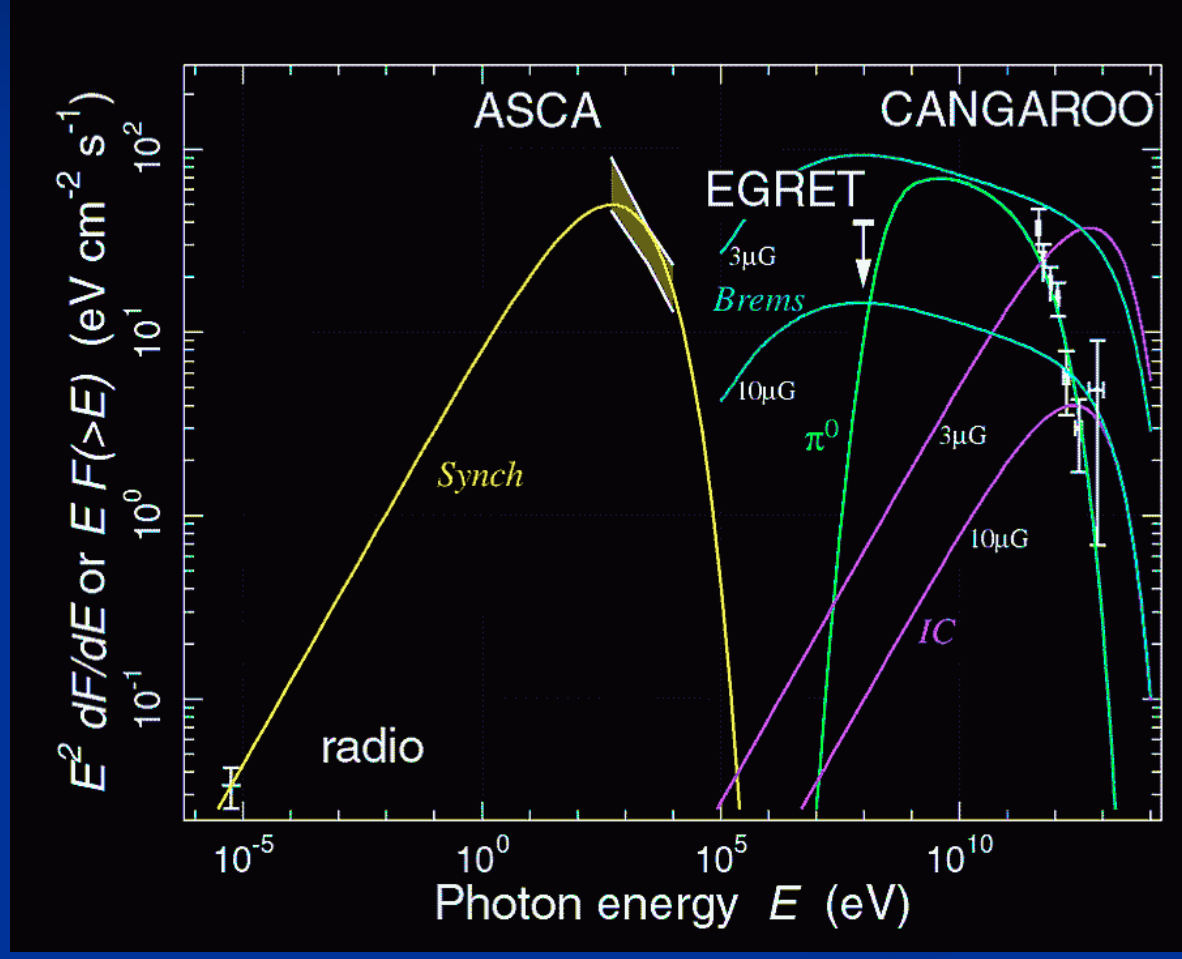


Significance map



Energy spectrum

# SNR RX J1713.7-3946 (2)



Hard to explain by emission from electrons (Brems, IC)

⇒ Emission from protons ( $\pi^0$ )?

⇒ Cosmic ray origin?

NANTEN results :

Distance  $\sim 1$  kpc

Age  $\sim 1600$  yr

→  $L_p \sim 10^{48} \text{ erg} \sim 0.001 L_{\text{SN}}$

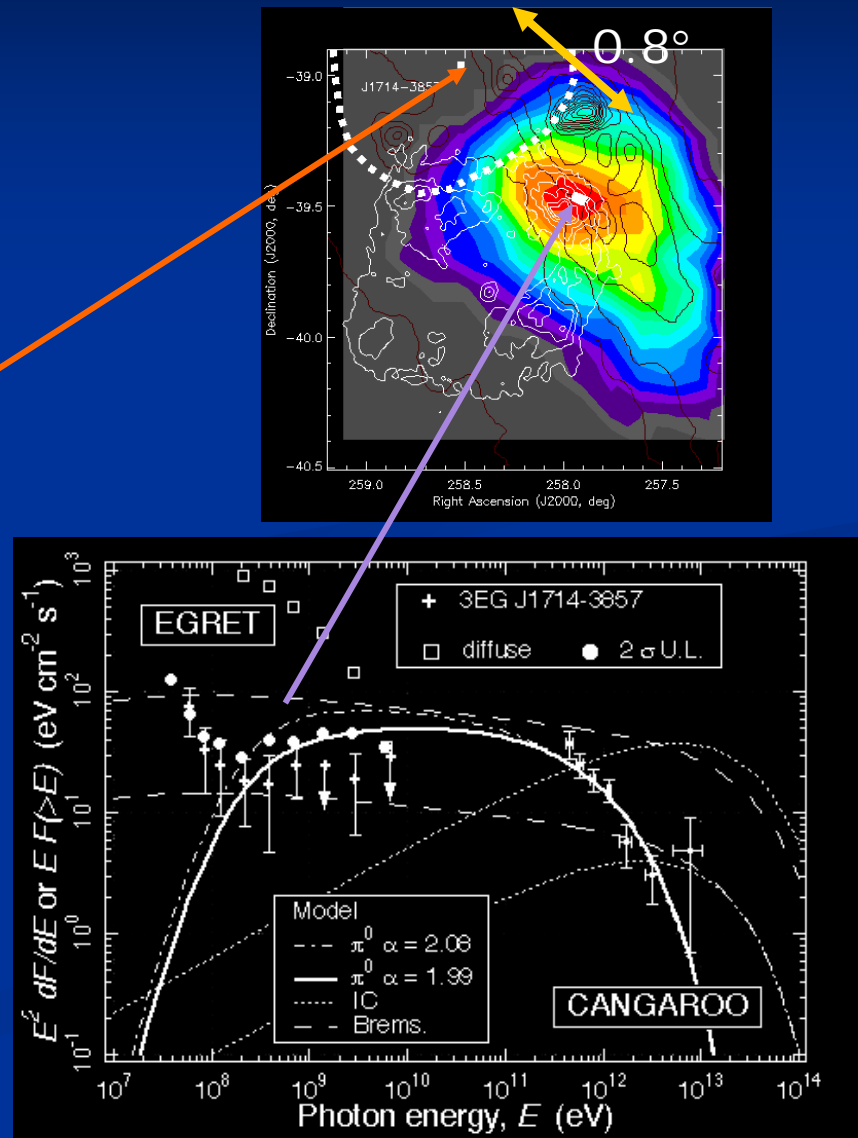
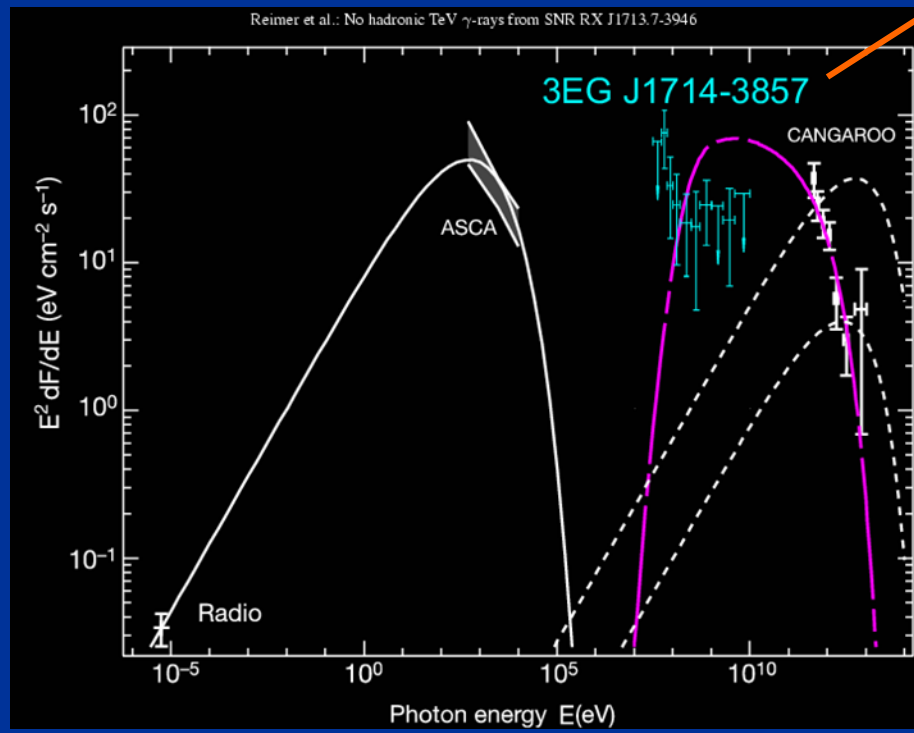
(Fukui et al. PASJ 55, 2003)

# SNR RX J1713.7-3946 (3)

Counter arguments

\* Reimer & Pohl, A&A 390 (2002) L43

\* Butt et al., Nature 418 (2002) 489



# SNR RX J1713.7-3946 (4)

F. Aharonian et al.: The  $\gamma$ -ray supernova remnant RX J1713.7-3946

9

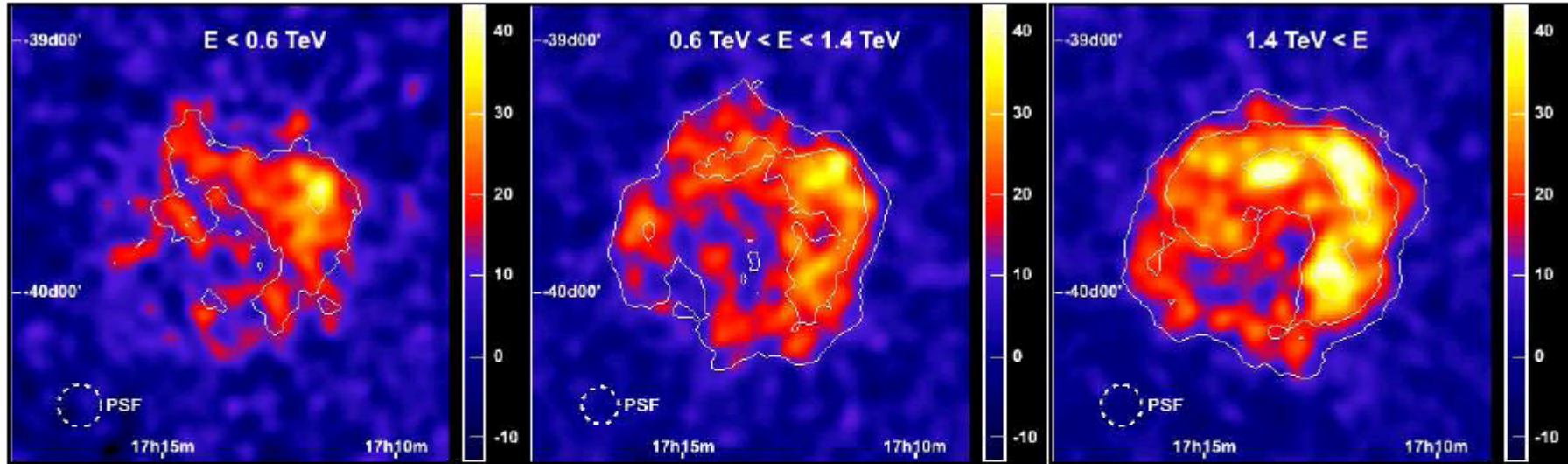


**Fig. 9.** Morphology of RX J1713.7–3946 as it appears at different energies. Shown from left to right are gamma-ray excess images with energies of  $E < 0.6 \text{ TeV}$ ,  $0.6 \text{ TeV} < E < 1.4 \text{ TeV}$ , and  $1.4 \text{ TeV} < E$ . Drawn additionally as white lines are contours of significance, linearly spaced at  $5, 10, 15\sigma$  (as in Fig. 7). Note the increase in the signal-to-noise ratio with increasing energy. The energy bands were chosen such that each band represents about a third of the full data set (taking events after cuts). Furthermore, all three images were smoothed with a Gaussian of  $2'$ , which makes them directly comparable to each other, and to Fig. 7. The resolution in each energy band is indicated in the lower left hand corner of the images; the three data subsets have comparable resolutions of  $\approx 0.08^\circ$  (the resolution of the intermediate energy band is about 6% better). This might be counter-intuitive, given that at larger energies camera images get bigger and fluctuation effects become negligible thereby improving the energy and direction resolution. However, in this case that effect is compensated by the increasing mean zenith angle of the large-energy events.

# SNR RX J1713.7-3946 (5)

CO

F. Aharonian et al.: The  $\gamma$ -ray supernova remnant RX J1713.7–3946

15

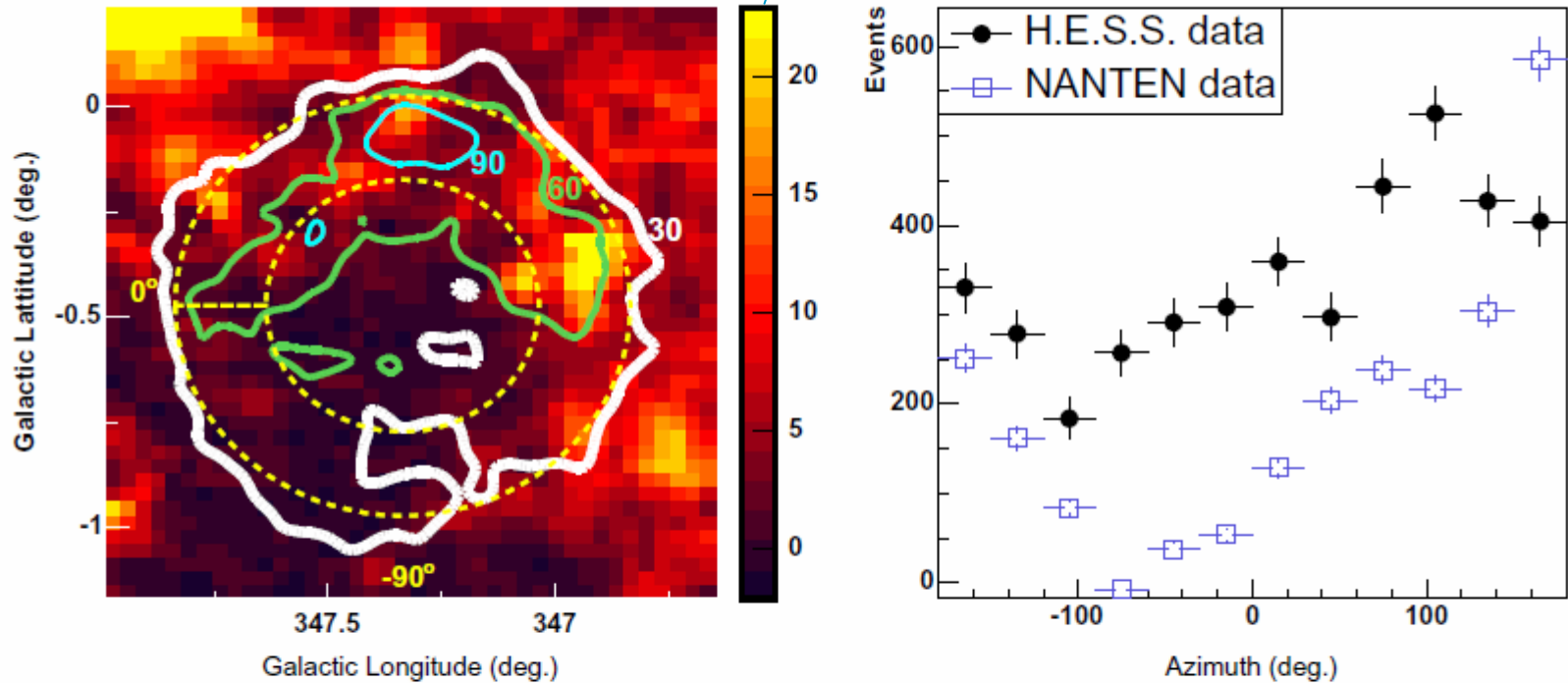


**Fig. 17.** Left panel: Shown are the intensity distribution of CO ( $J = 1 - 0$ ) emission (Fukui et al. 2003) (linear colour scale in units of  $K \text{ km s}^{-1}$ , truncated at a value of 23 to highlight important features), derived by integrating the CO spectra in the velocity range from  $-11 \text{ km s}^{-1}$  to  $-3 \text{ km s}^{-1}$  (which corresponds to 0.4 kpc to 1.5 kpc in space). Overlaid are coloured contours of the H.E.S.S. gamma-ray excess image. The levels are labelled and linearly spaced at 30, 60, and 90 counts. Note that the image is shown in Galactic coordinates. Right panel: Azimuth profile plot, that is, number of counts as a function of the azimuthal angle, integrated in a  $0.2^\circ$ -wide ring covering the shell of RX J1713.7–3946 (dashed yellow circle in the left-hand panel). Plotted are the H.E.S.S. gamma-ray and the NANTEN data set.

# SNR RX J1713.7-3946 (6)

Electron origin model

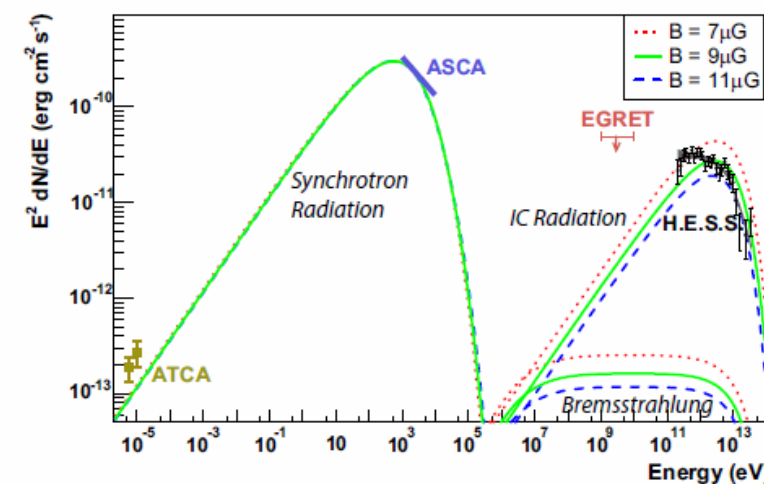


Fig. 19. Broadband SED of RX J1713.7–3946. The ATCA radio data and ASCA X-ray data (Hiraga 2005) for the whole SNR are indicated, along with the H.E.S.S. measurement and the EGRET upper limit. Note that the radio flux was determined in Lazendic et al. (2004) for the northwest part of the shell only and was scaled up by a factor of two here to account for the whole SNR. The synchrotron and IC spectra were modelled assuming a source distance of 1 kpc, an age  $T$  of 1000 years, a density  $n$  of  $1 \text{ cm}^{-3}$ , and a production rate of relativistic electrons by the acceleration mechanism in the form of a power law of index  $\alpha = 2$  and an exponential cutoff of  $E_0 = 100 \text{ TeV}$ . Shown are three curves for three values of the mean magnetic field:  $7 \mu\text{G}$ ,  $9 \mu\text{G}$ , and  $11 \mu\text{G}$ , to demonstrate the required range of the B field strength for this scenario. The electron luminosity is adopted such that the observed X-ray flux level is well matched. For the three magnetic field values the luminosity  $L_e$  is  $L_e = 1.77 \times 10^{37} \text{ erg s}^{-1}$  ( $7 \mu\text{G}$ ),  $L_e = 1.14 \times 10^{37} \text{ erg s}^{-1}$  ( $9 \mu\text{G}$ ), and  $L_e = 0.81 \times 10^{37} \text{ erg s}^{-1}$  ( $11 \mu\text{G}$ ).

Proton origin model

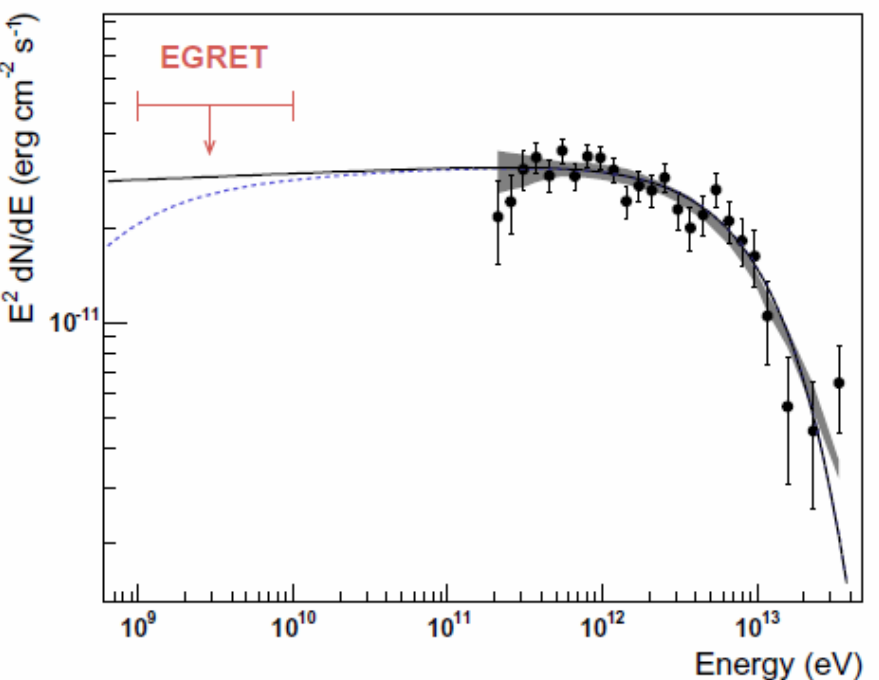
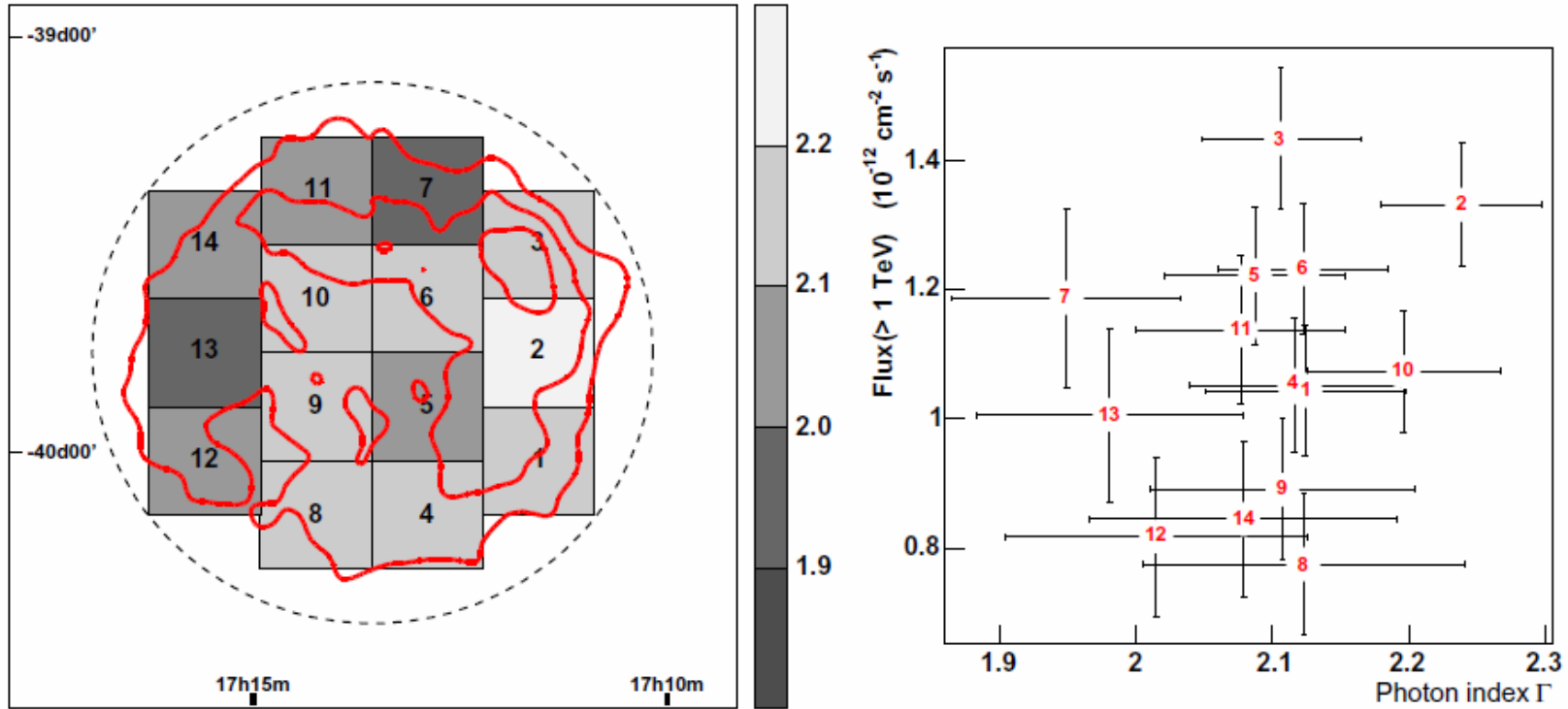


Fig. 20. H.E.S.S. data points plotted in an energy flux diagram. They shaded grey band is the systematic error band for this measurement (see Sect. 3.2). The black curve is the best fit of a power law with exponential cutoff to the data, extrapolated to lower energies. The dashed blue curves is the same function, but it takes the  $\pi^0$  kinematics into account. The EGRET upper limit from 1 GeV to 10 GeV is plotted as red arrow.

⇒ Protons favored (?)

# SNR RX J1713.7-3946 (7)



**Fig. 14.** The image illustrates the results of the spatially resolved spectral analysis. **Left part:** Shown in red are gamma-ray excess contours from Fig. 7, linearly spaced at 30, 60, and 90 counts. Superimposed are the 14 boxes (each  $0.26^\circ \times 0.26^\circ$  in dimension) for which spectra were obtained independently. The dashed line is the  $0.65^\circ$  radius circle that was used to integrate events to produce a spectrum of the whole SNR. The photon index obtained from a power-law fit in each region is colour coded in bins of 0.1. The ranges of the fits to the spectra have been restricted to a maximum of 8 TeV (see Table 2). **Right part:** Plotted is the integral flux above 1 TeV against the photon index, for the 14 regions the SNR was sub-divided in. The error bars are  $\pm 1\sigma$  statistical errors. Note that systematic errors of 25% on the flux and 0.1 on the photon index are to be assigned to each data point additionally.

# SNR RX J0852.0-4622 [G266.2-1.2, Vela Jr.](1)

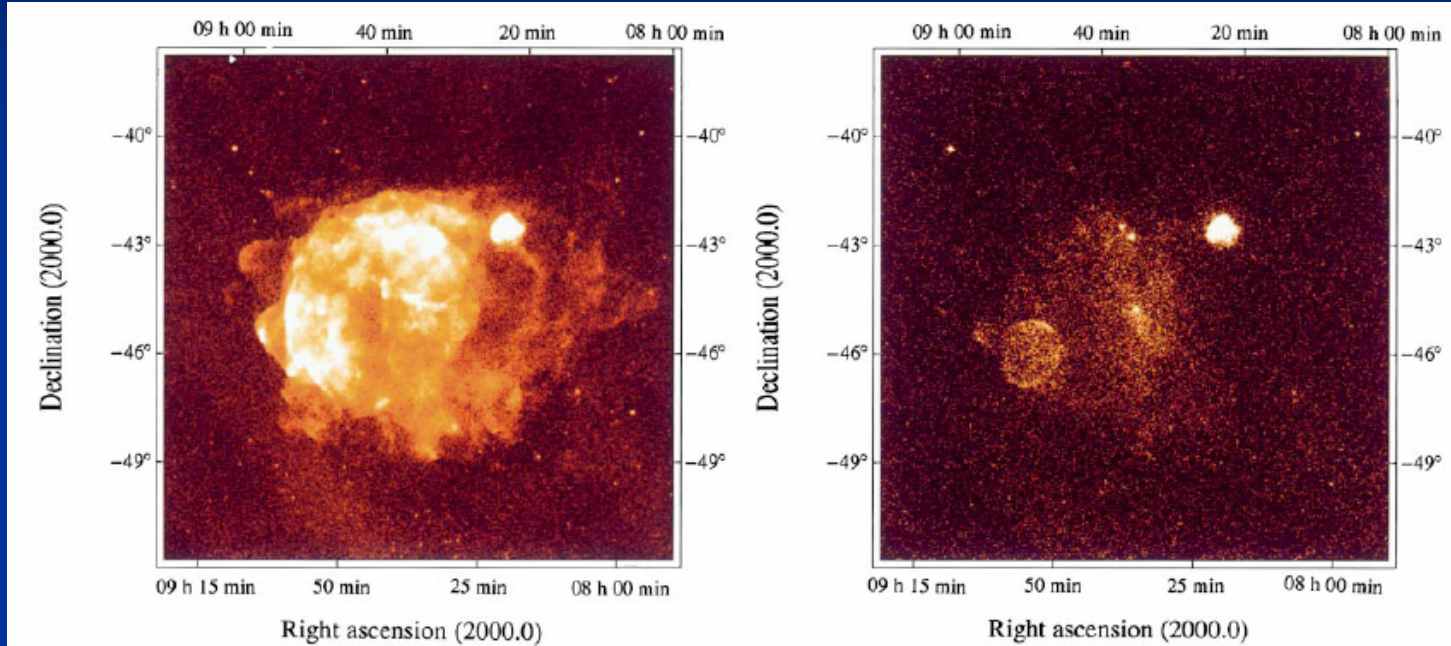
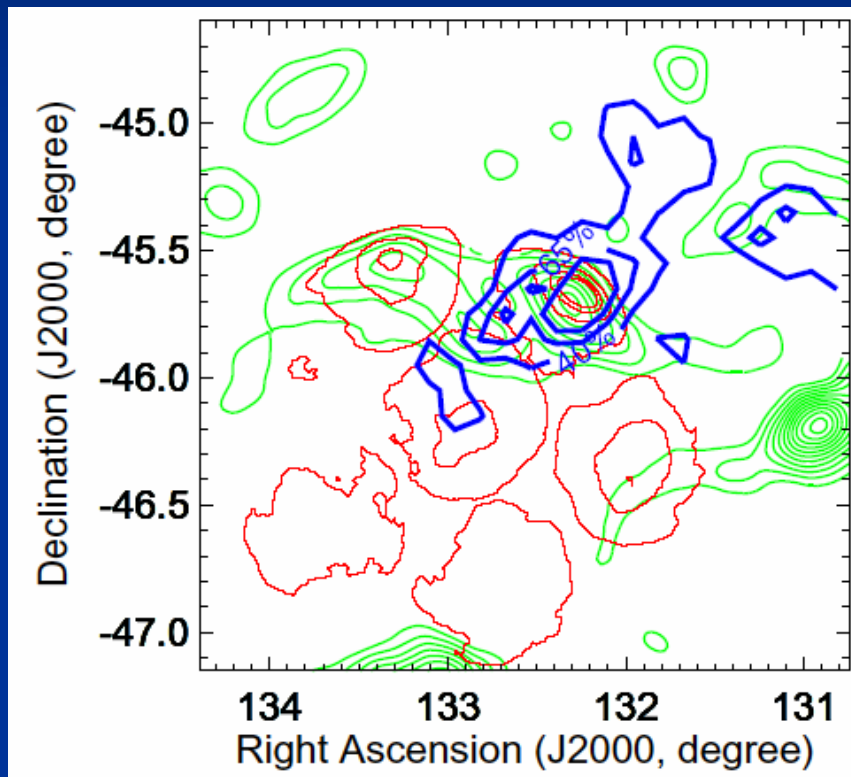


**Figure 1** Rosat all-sky survey images of the Vela SNR and its surroundings. Angular resolution is 1 arcmin half-power radius; mean exposure is 993 s. The left-hand image was taken for photon energies  $0.1 < E < 2.4$  keV; surface brightness increases from dark yellow to white by a factor of 500. The right-hand image is for photon energies  $>1.3$  keV. Most of the Vela SNR X-ray emission which dominates at low energies had disappeared. At the centre, the synchrotron nebula around the Vela pulsar remains visible as well as the SSW beam-like structure, and at the very northwest (upper right) the bright Puppis-A SNR can be seen. The new shell-type SNR RX J0852.0 – 4622 shows up in the lower left. East of RX J0852.0 – 4622 hard X-ray photons from the D/D' Vela SNR shrapnels are seen which, however, are associated with a much lower-temperature spectrum than RX J0852.0 – 4622 (ref. 14). For X-ray spectral analysis, RX J0852.0 – 4622 was divided into two

regions, one containing the bright northern limb section (l) and the other one (r) excluding the northern and southern limbs. Spectral fits were performed with either power-law models, optically thin thermal emission equilibrium models (Raymond-Smith models) or combinations of both. Solutions with a reduced  $\chi^2 < 1$  for region r are obtained only with a two-temperature model with  $kT_{t,1} = 0.14^{+0.08}_{-0.08}$  keV,  $kT_{t,2} = 2.5^{+4.5}_{-0.7}$  keV. The spectrum of the northern limb can be fitted by either a simple power law with index  $\alpha = -2.6^{+0.3}_{-0.4}$  or a two-temperature model with  $kT_{l,1} = 0.21^{+0.14}_{-0.09}$  keV,  $kT_{l,2} = 4.7^{+4.5}_{-0.7}$  keV. The presence of low-temperature components may partially be due to a residual, uncorrected contribution from the much softer Vela SNR. The total, absorption-corrected flux of the high-temperature components is  $F_x(0.1\text{--}2.4\text{ keV}) = 3 \times 10^{-10}$  erg cm $^{-2}$  s $^{-1}$ .

# SNR RX J0852.0-4622 (2)



CANGAROO-II: Katagiri et al.,  
ApJ, 619, (2005) L163

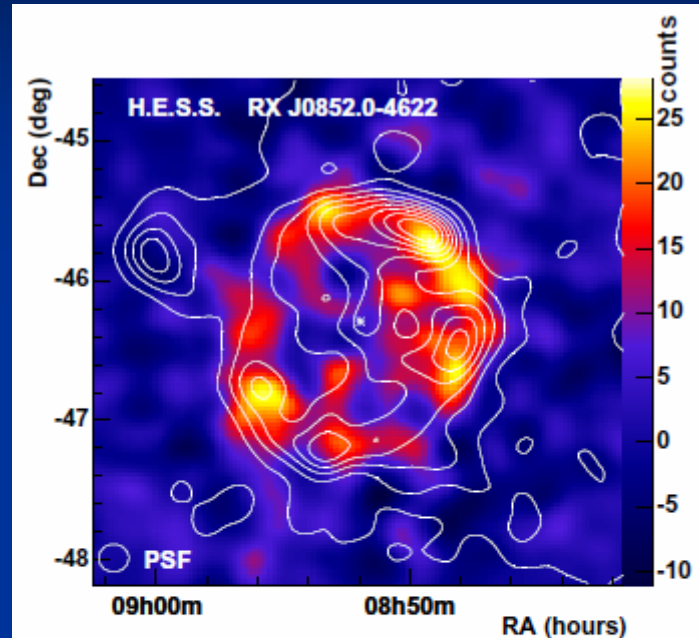
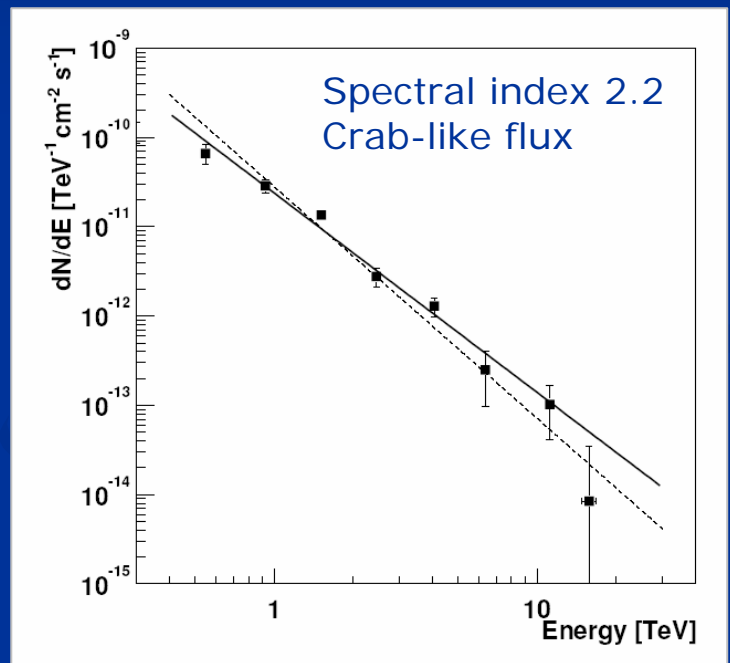
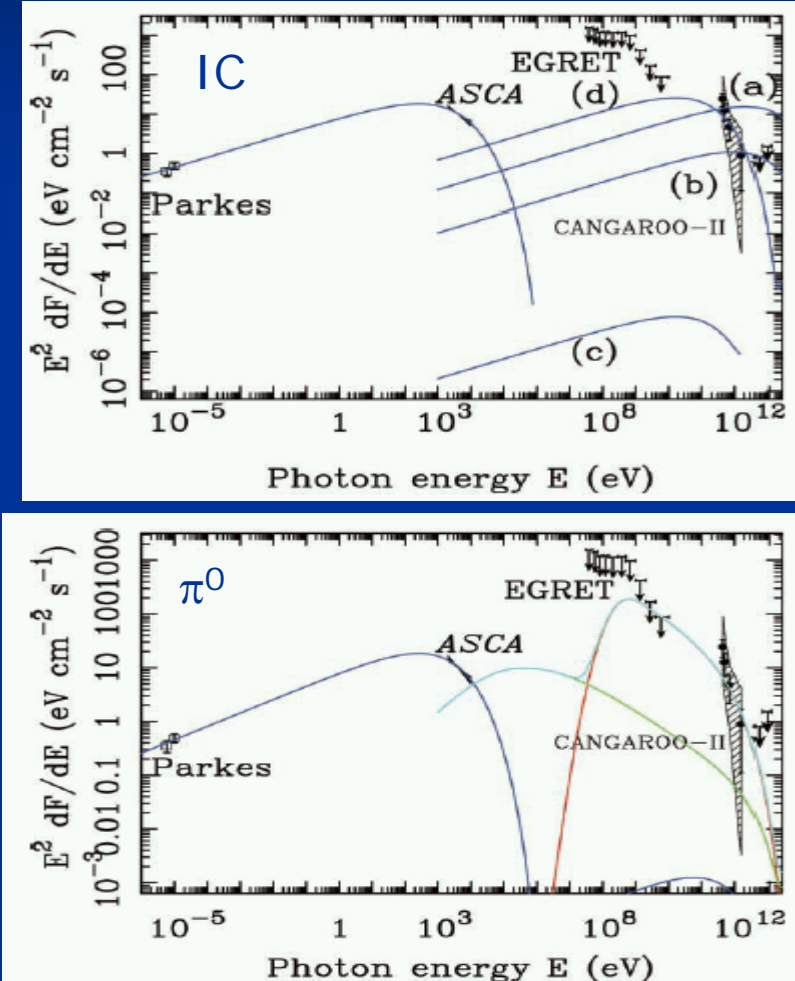


Fig. 2. Count map of  $\gamma$ -rays from the direction of RX J0852.0-4622 after background subtraction. The data are smoothed with a Gaussian ( $\sigma = 0.1^\circ$ ) representing the angular resolution of the instrument. The point spread function (PSF) is indicated by a circle.  $\gamma$ -ray features smaller than the PSF should not be considered as real. The lines denote equidistant contours of smoothed ( $\sigma = 0.1^\circ$ ) X-ray data from the ROSAT All Sky Survey, with energies restricted to above 1.3 keV. The position of the neutron star candidate AX J0851.9-4617.4 is marked with an asterisk. The axes show J2000.0 equatorial coordinates.

H.E.S.S.: Aharonian et al., AA  
437, L7 (2005)

# SNR RX J0852.0-4622 (3)



H.E.S.S. (Hofmann,  
Cherenkov2005)

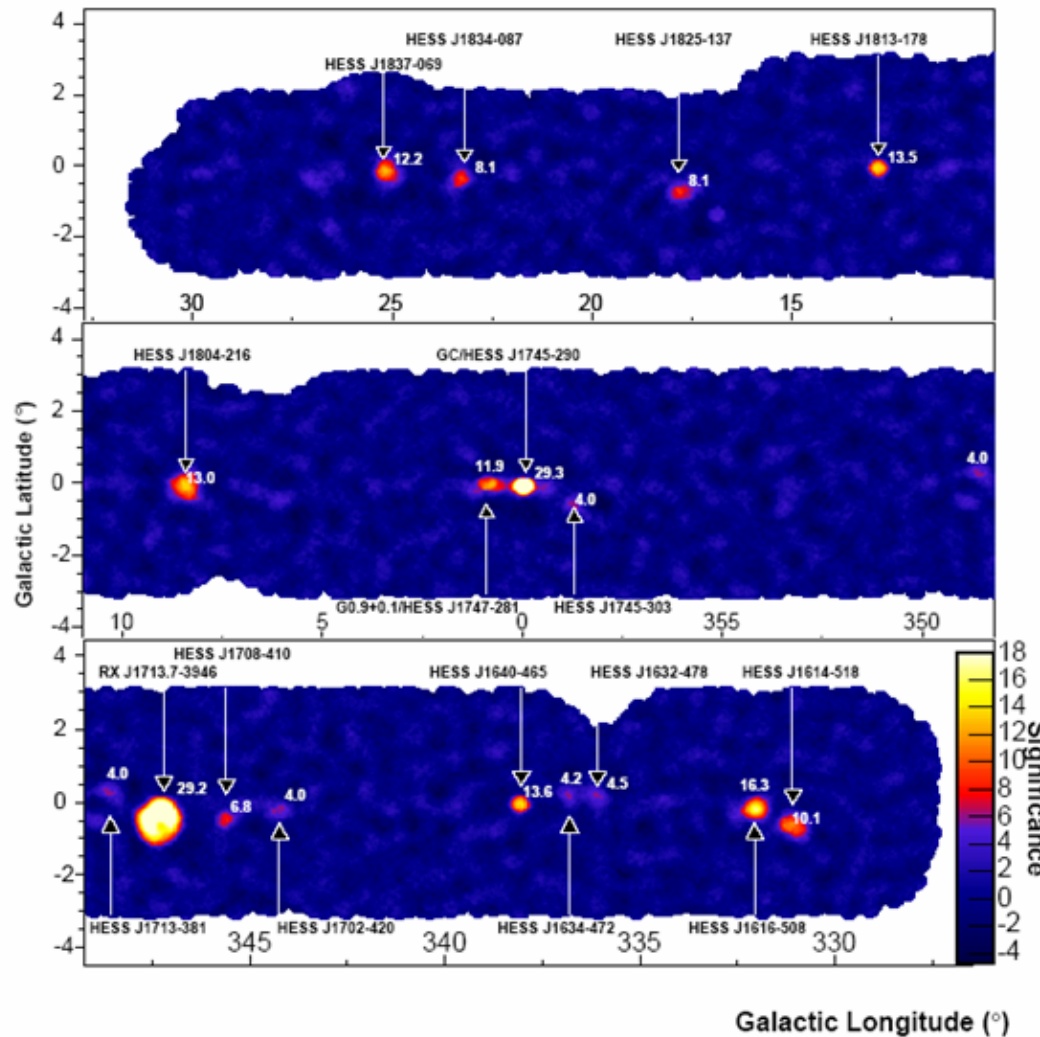
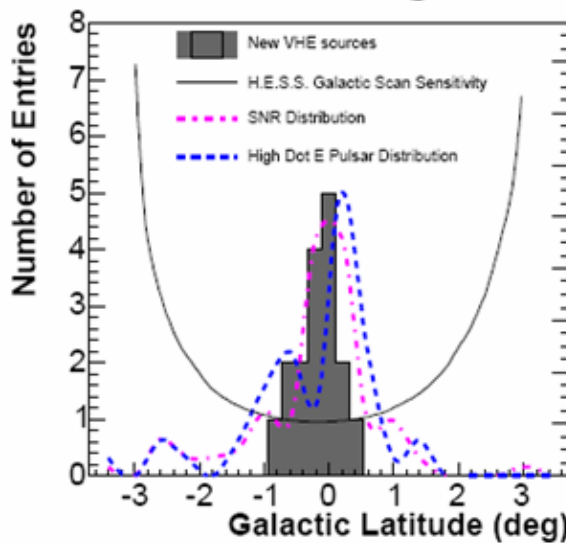
CANGAROO-II: Katagiri et al., ApJ, 619,  
(2005) L163

# H.E.S.S. Highlight: Galactic Plane Survey

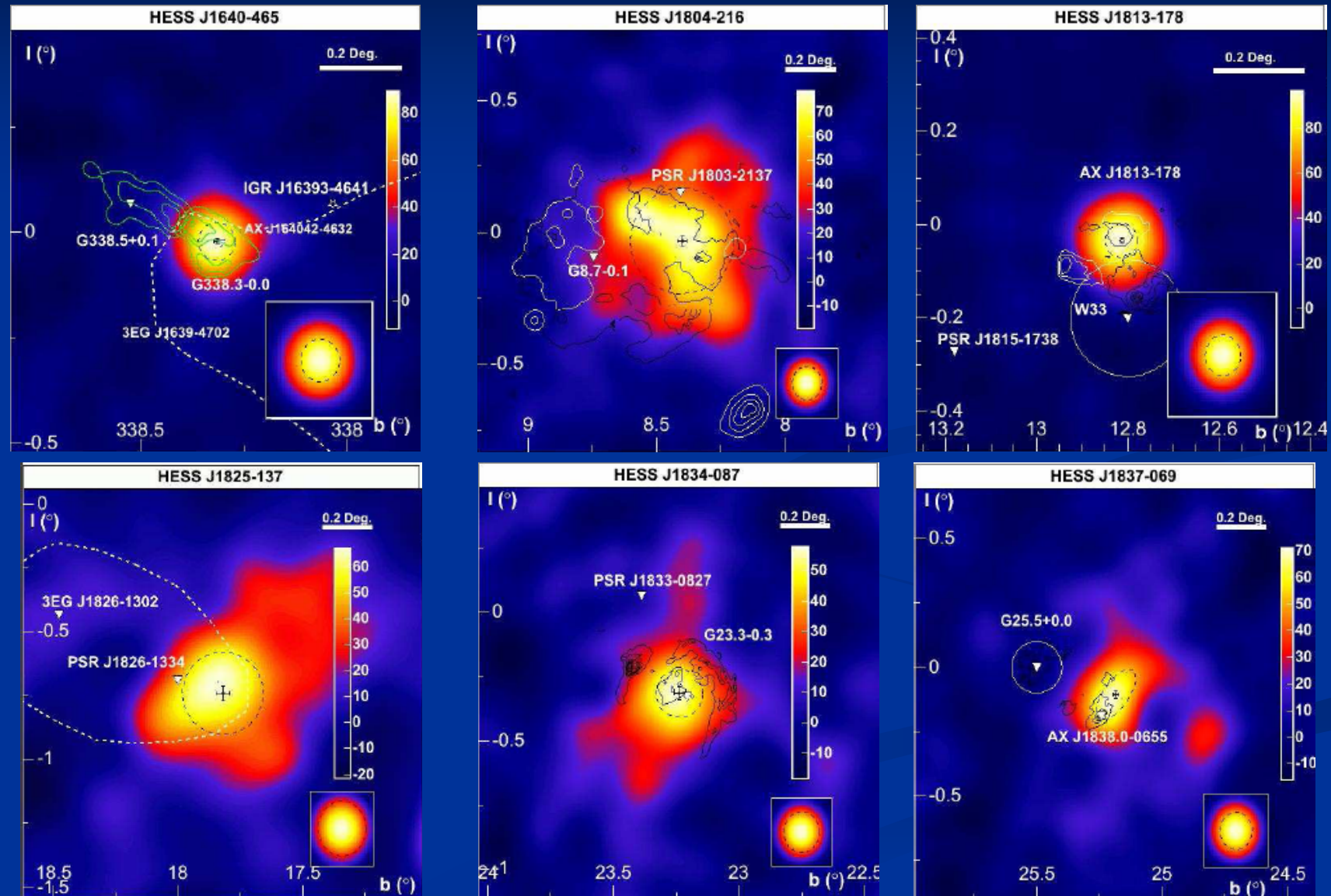
► S. Funk, OG 23  
► A. Lemiere, OG 23

15 new TeV sources  
+ 3 known

Scale height:  
 $\approx 0.3^\circ$  rms  
 $\approx$  molecular gas



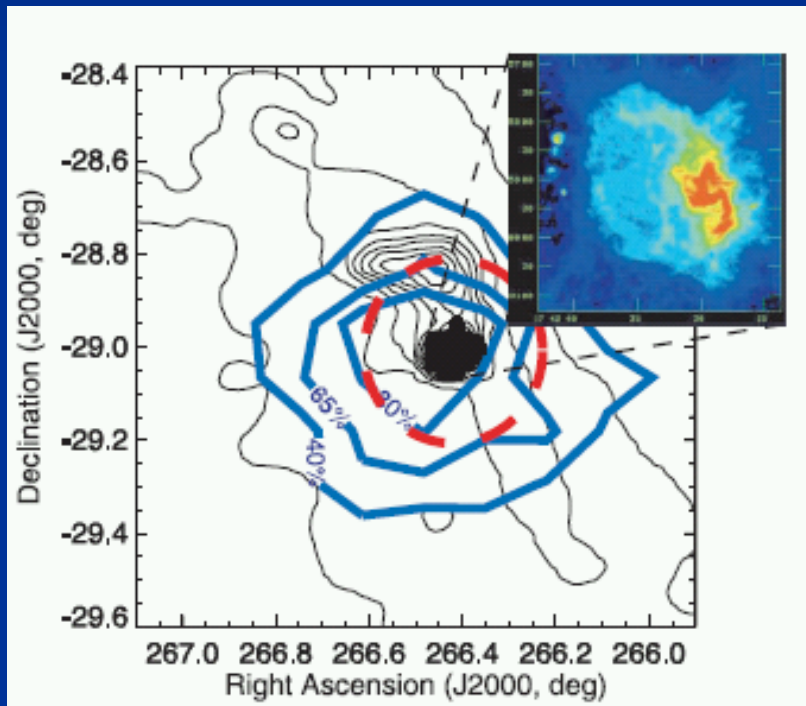
# Other SNRs?



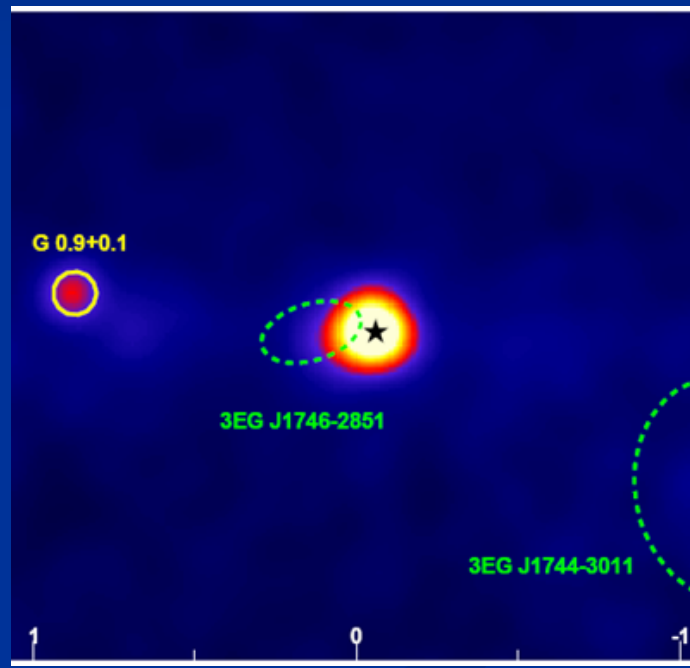
# “New” galactic sources

- The Galactic center
  - Whipple 2004, CANGAROO 2004, H.E.S.S. 2004
- Pulsar wind nebulae
  - MSH15-52 [CANGAROOH.E.S.S. 2005]
  - Vela X [H.E.S.S. 2005]
- Pulsar binary PSR 1259-63/SS2883
  - H.E.S.S. 2005
- X-ray binary/microquasar LS5039
  - H.E.S.S. 2005
- UnID
  - HEGRA J2032+4130
  - H.E.S.S. J1303-631

# The Galactic center [Sgr A\*]



CANGAROO-II (Tsuchiya et al., ApJ 606, L115, 2004)



H.E.S.S.: W.Hofmann,  
ICRC2005

# Dark matter signal from Sgr A\*?

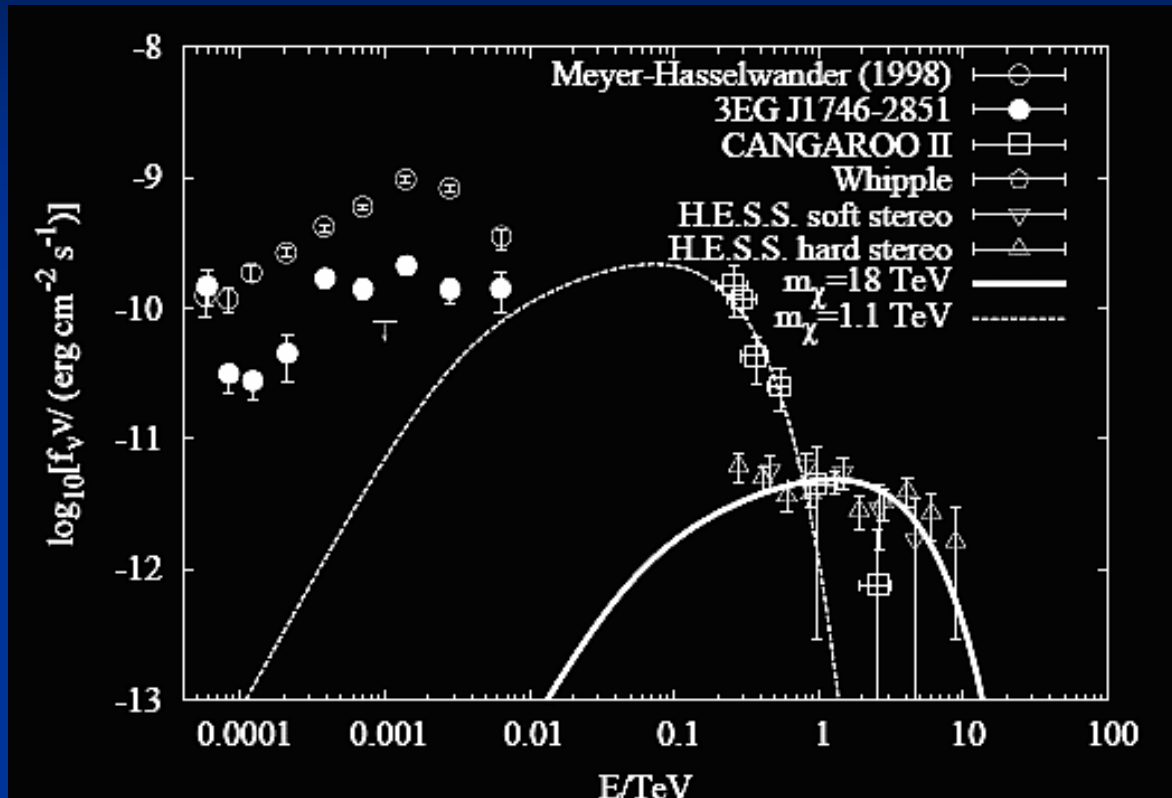
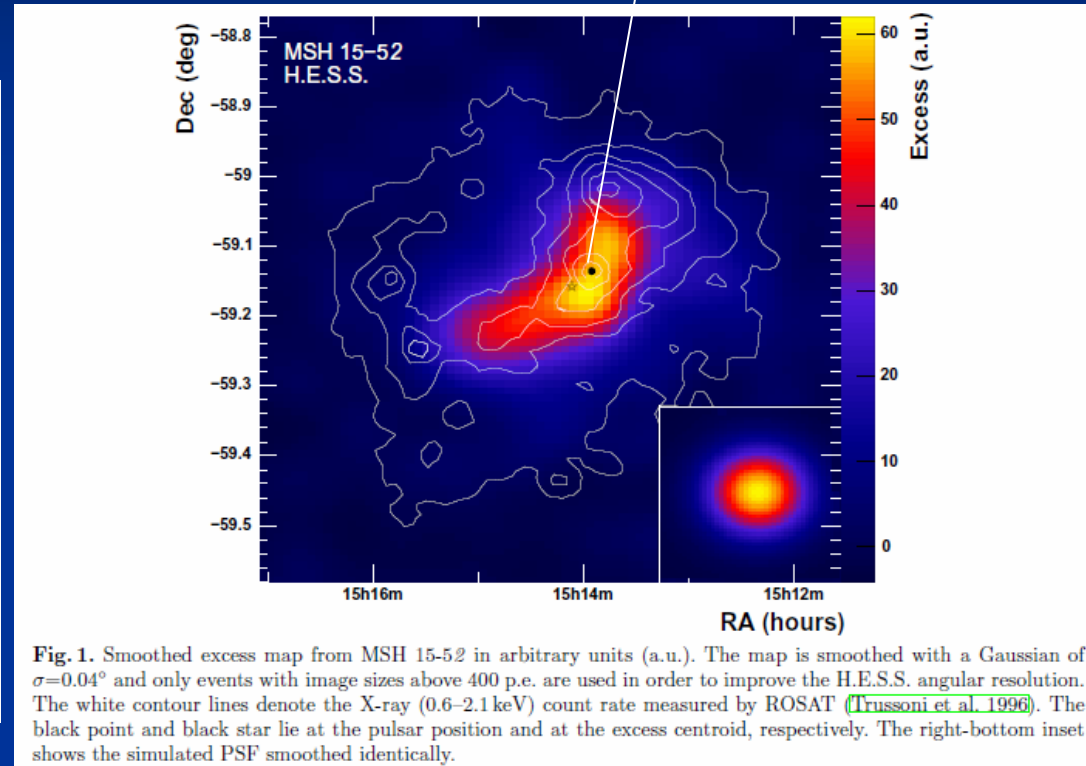
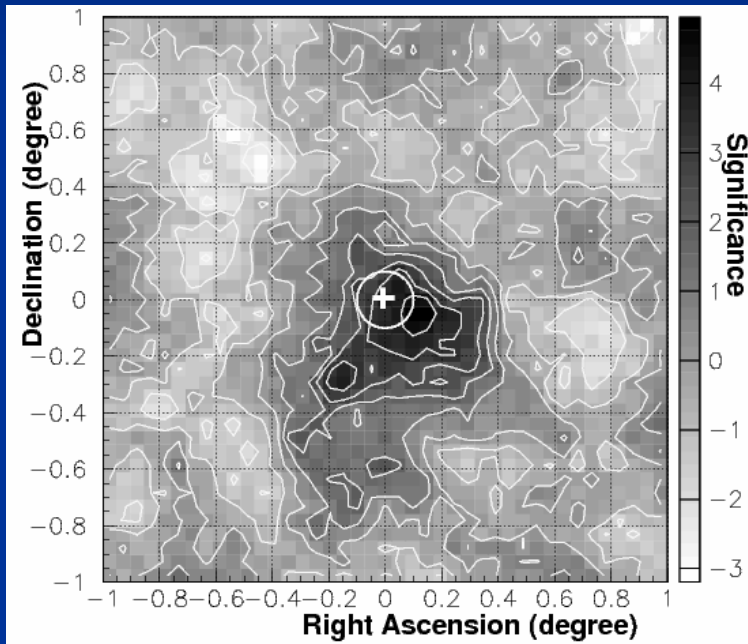


Fig. 2. A summary of data and best-fit models for WIMP annihilation from the Galactic center: H.E.S.S. (open triangles), CANGAROO (open boxes), EGRET (solid and open circles), 10m Whipple telescope of the VERITAS collaboration (solid diamond).

# Pulsar wind nebula MSH15-52



CANGAROO-I.:

Sako et al., ApJ 537, 422 (2000)

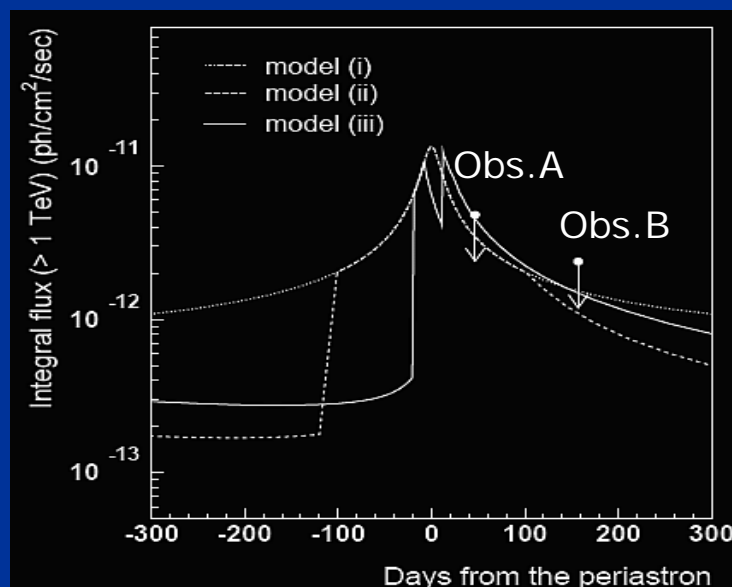
H.E.S.S.:

Aharonian et al., A&A 435, L17 (2005)

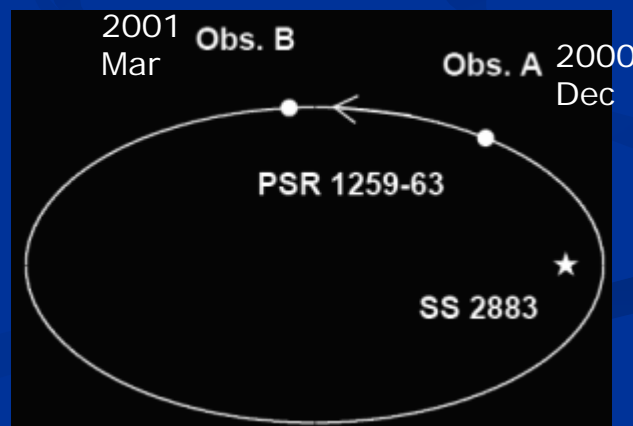
# Pulsar binary PSR 1259-63/SS2883 (1)



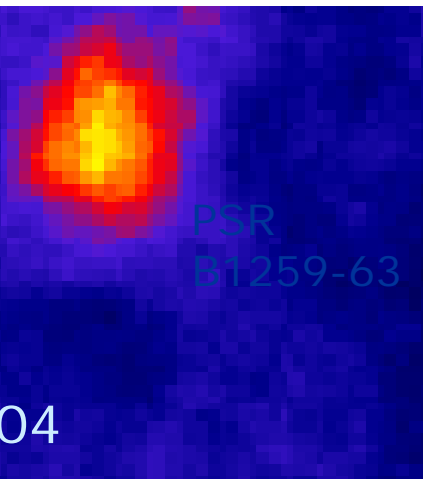
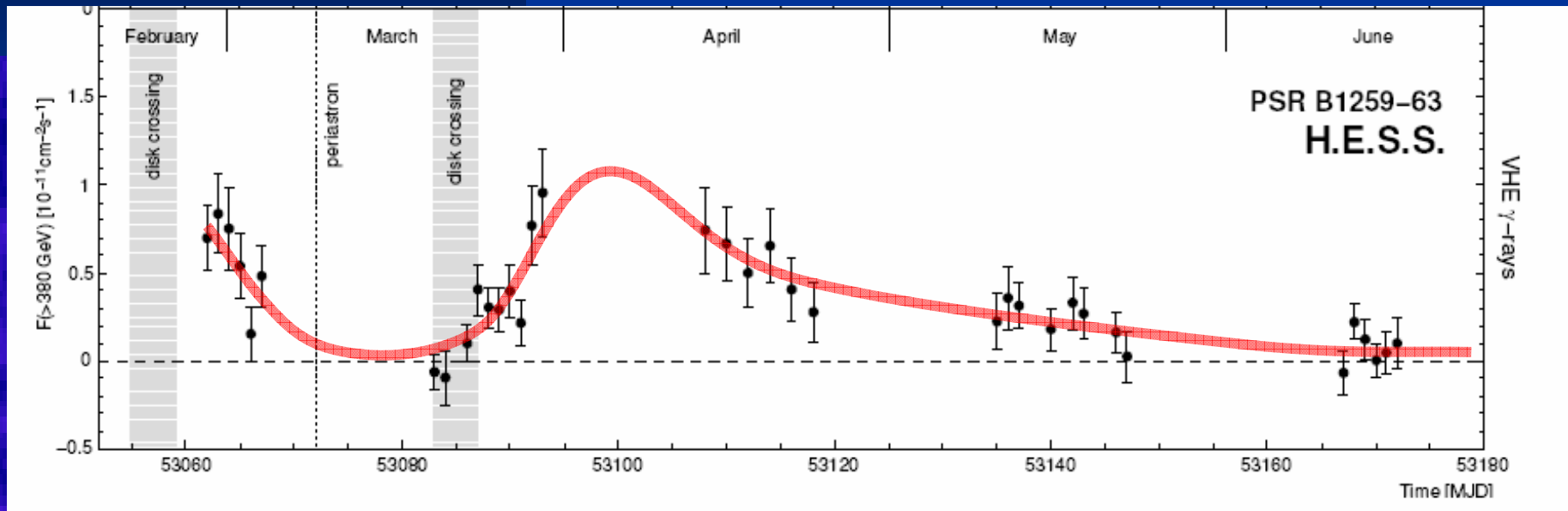
3.4 year highly eccentric orbit around  $\sim 10 M_{\odot}$   
Be star closest approach  $\sim 10^{13} \text{ cm}$  or  $\sim 20$  stellar radii



- (i) aligned disc to the orbital plane and interaction throughout the orbit
- (ii) mis-aligned disc and interaction in the  $\sim 200$ -day period around periastron ( $\tau$ ), during which the radio emission is depolarized
- (iii) mis-aligned disc and interaction in two short periods,  $[(\tau - 18 \text{ d}) \sim (\tau \sim -8 \text{ d})]$  and  $[(\tau + 12 \text{ d}) \sim (\tau + 22 \text{ d})]$

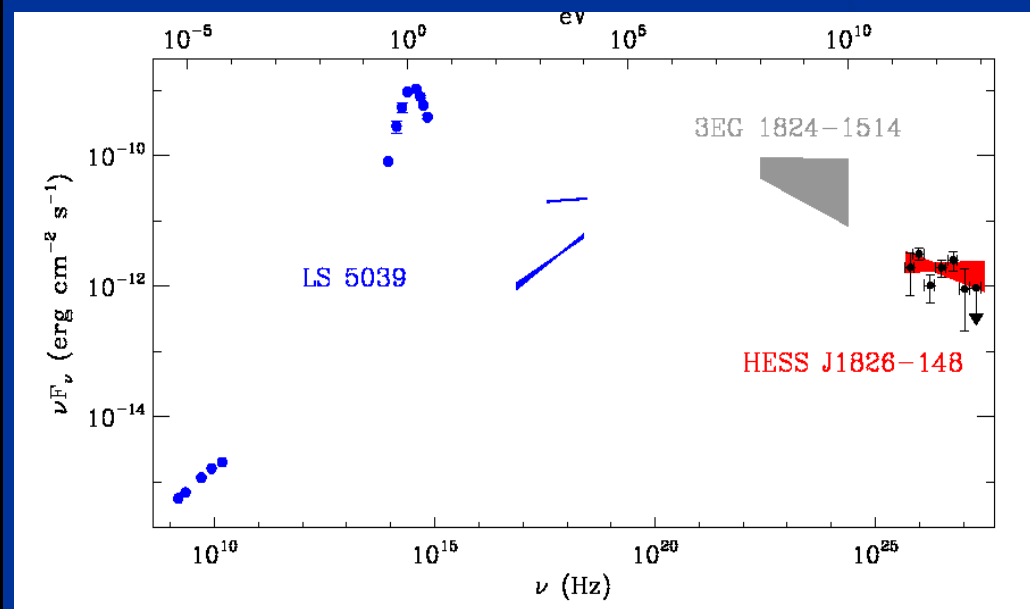
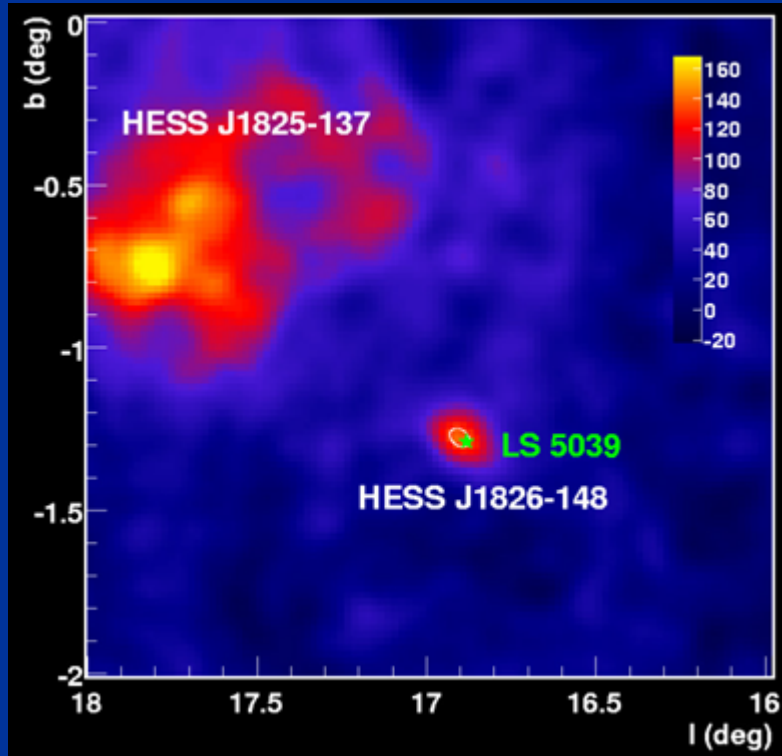


# Pulsar binary PSR 1259-63/SS2883 (2)



# X-ray binary/microquasar LS5039

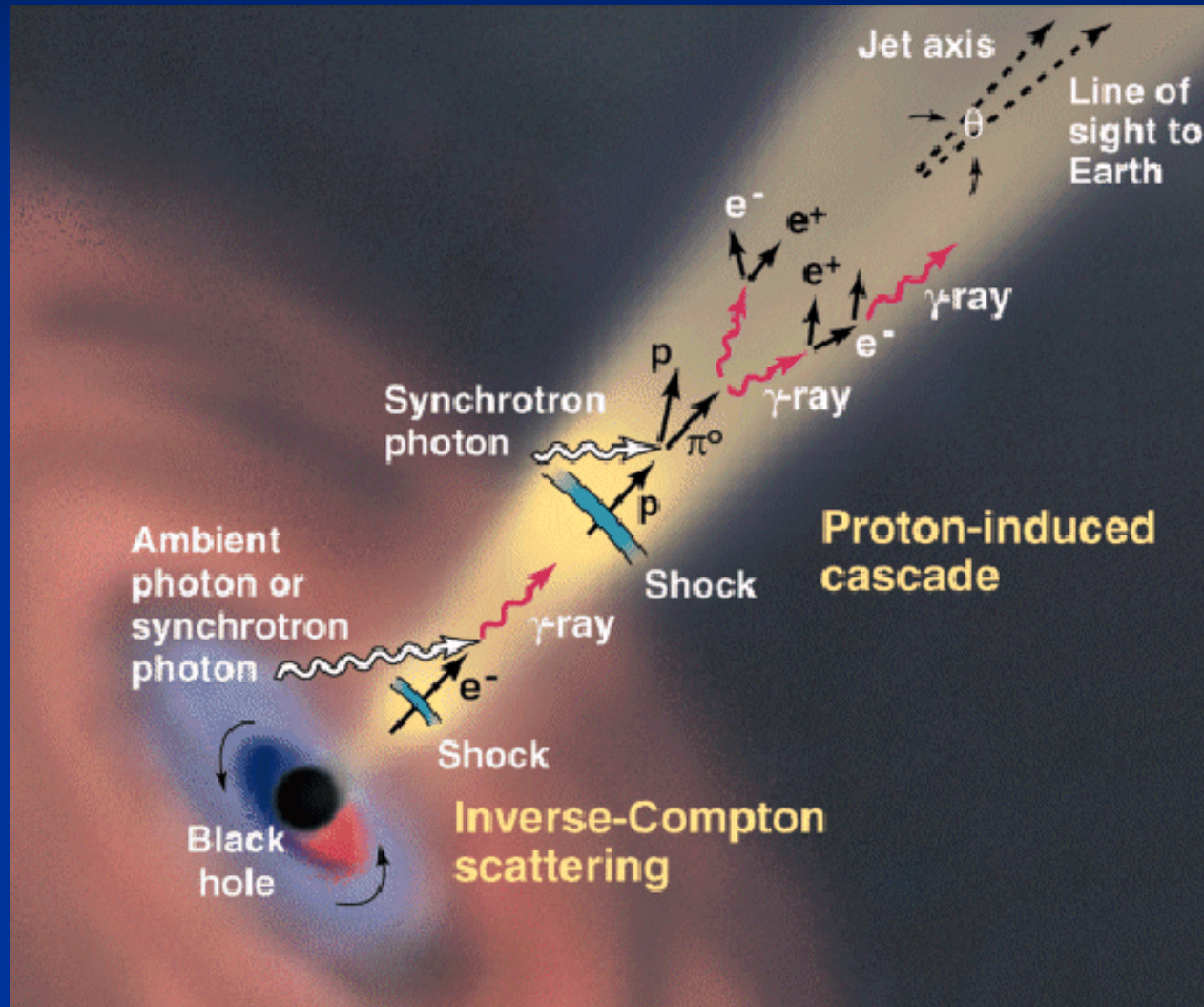
- compact 4 (?)  $M_{\odot}$  object in eccentric 4 day orbit around 20-30  $M_{\odot}$  star
- closest approach  $\sim 10^{12}$  cm or  $\sim 2$  stellar radii



# Extragalactic sources: basics

- Active galactic nuclei
  - Blazars
    - Wide-band spectrum – nonthermal
    - Quasars – LBL (RBL) – HBL (XBL) sequence
    - Leptonic models
      - SSC or EC (External Compton)
    - Hadronic models
      - Proton-initiated cascades
  - Radio galaxy,...
- Gamma-ray absorption by EBL (Extragalactic Background Radiation)
  - Infrared photon field: uncertain
- Center of galaxies
  - Accumulation of dark matter??
- Extragalactic background radiation

# Blazars



Beaming factor

$$\delta \equiv 1/\Gamma (1 - \beta \cos \theta) > 1$$

Observed frequency

$$\nu \propto \nu_0 \delta$$

Apparent luminosity

$$L \propto L_0 \delta^4$$

# “Known” extragalactic sources

- Mrk421 ( $z=0.031$ )
  - First detection in 1992 [Punch et al. Nature 1992]
  - Flares in 1994, 1996, 2001, 2002-3
- Mrk501 ( $z=0.034$ )
  - First detection in 1995 [Quinn et al. ApJ 1996]
  - Large flares in 1997
- 1H1426+428 ( $z=0.129$ )
  - First detection in 2001 [Horan et al. 5<sup>th</sup> Compton 2001]
  - Flares in 2001

# Multiwavelength spectra of blazars

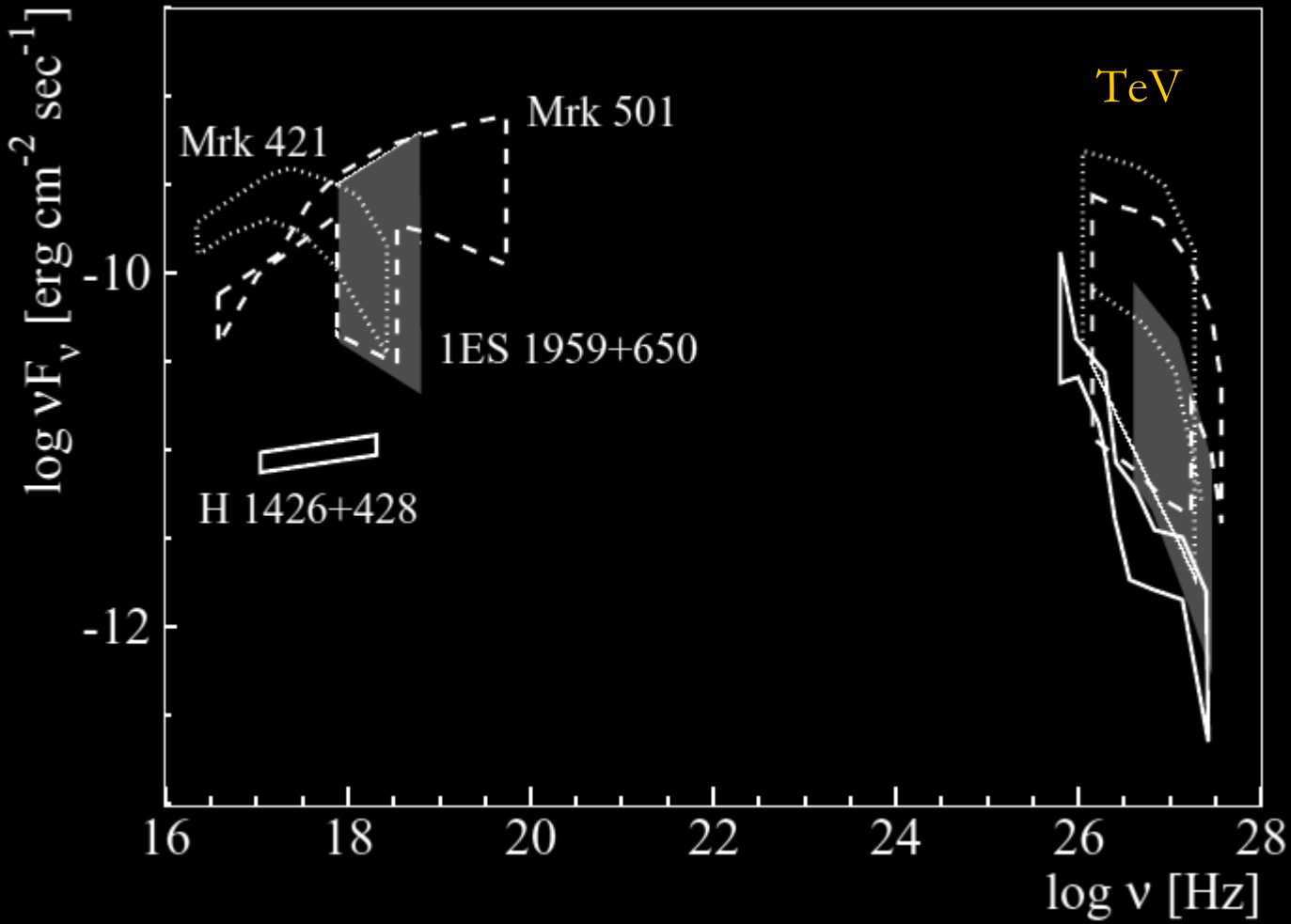


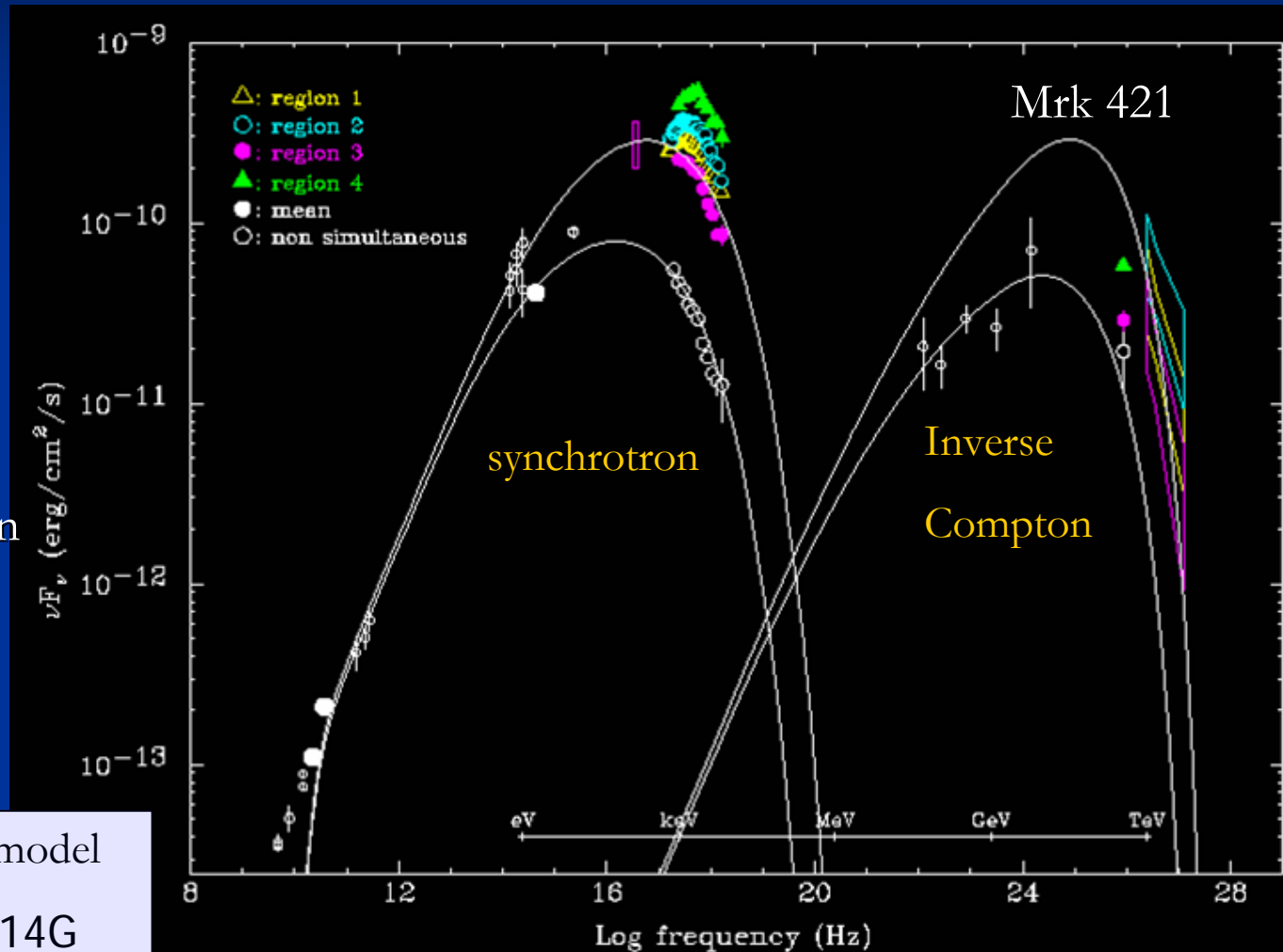
Fig. 1. Simultaneous and non-simultaneous X-ray and TeV  $\gamma$ -ray energy spectra of the 4 TeV blazars with measured TeV  $\gamma$ -ray energy spectra. The regions show the range of values that have been observed with BeppoSAX, RXTE and Cherenkov Telescopes (from (46)).

# Synchrotron self-Compton model

- Synchrotron + inverse Compton model works well  
→  $e^\pm$  origin (SSC: Synchrotron Self Compton)

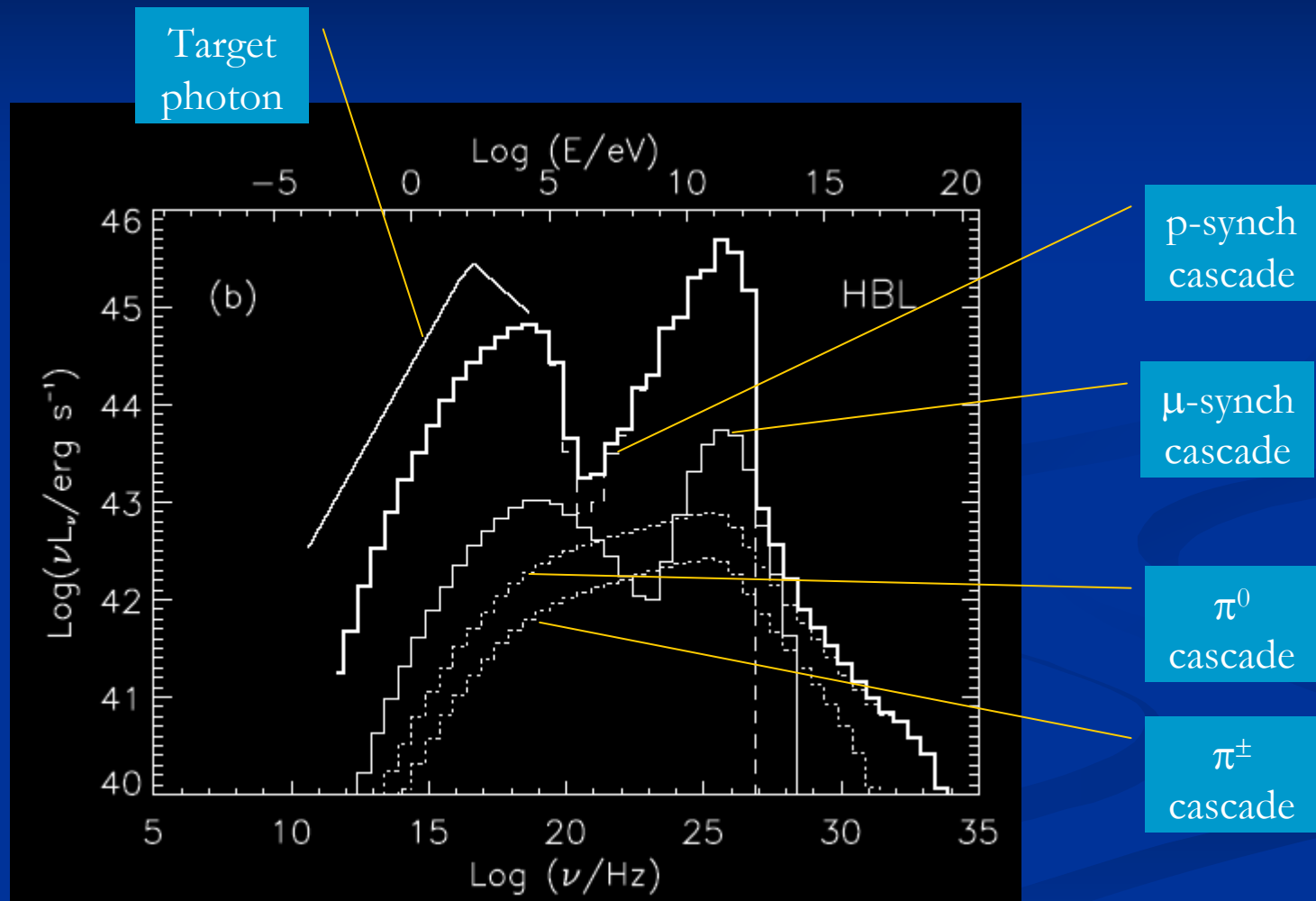
One-zone SSC model

$$\delta = 14, B = 0.14 \text{ G}$$

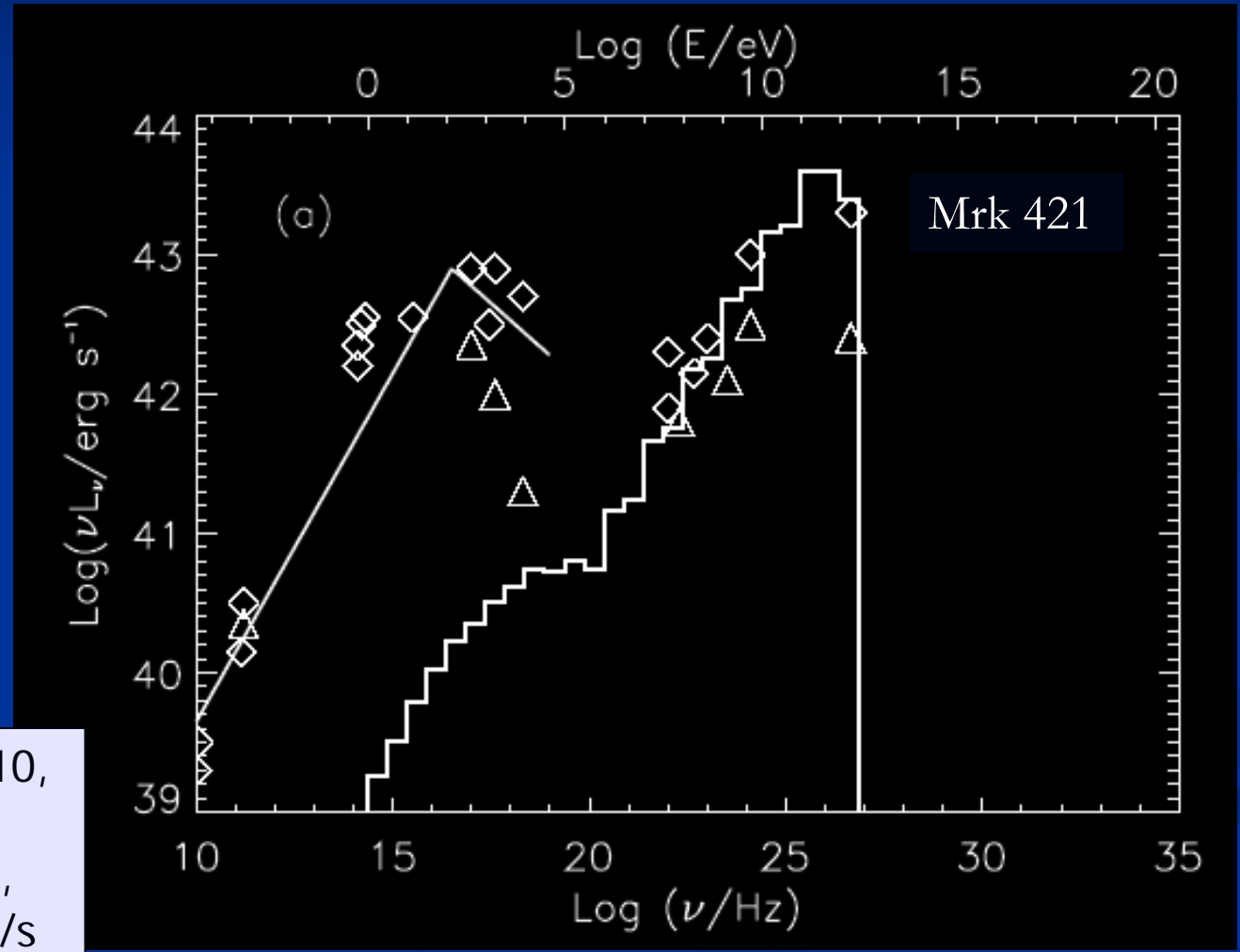


Takahashi et al. ApJ 542, 2000

# Synchrotron proton blazar model (1)

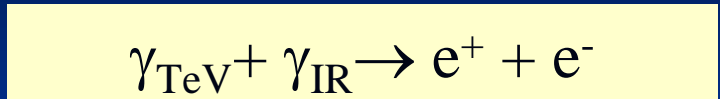
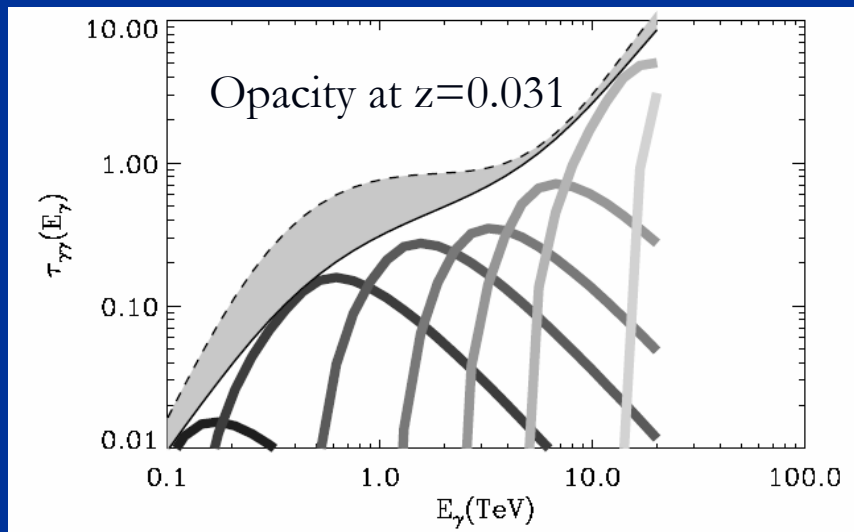
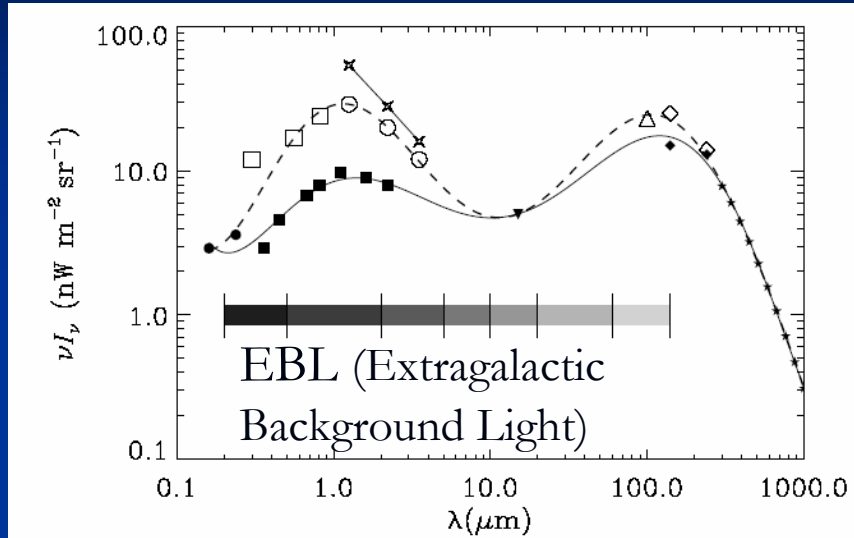


# Synchrotron proton blazar model (2)



Muecke et al. APh 18, 2003

# TeV gamma-ray absorption on EBL (1)



Mean free path for  $e^+e^-$  pair production

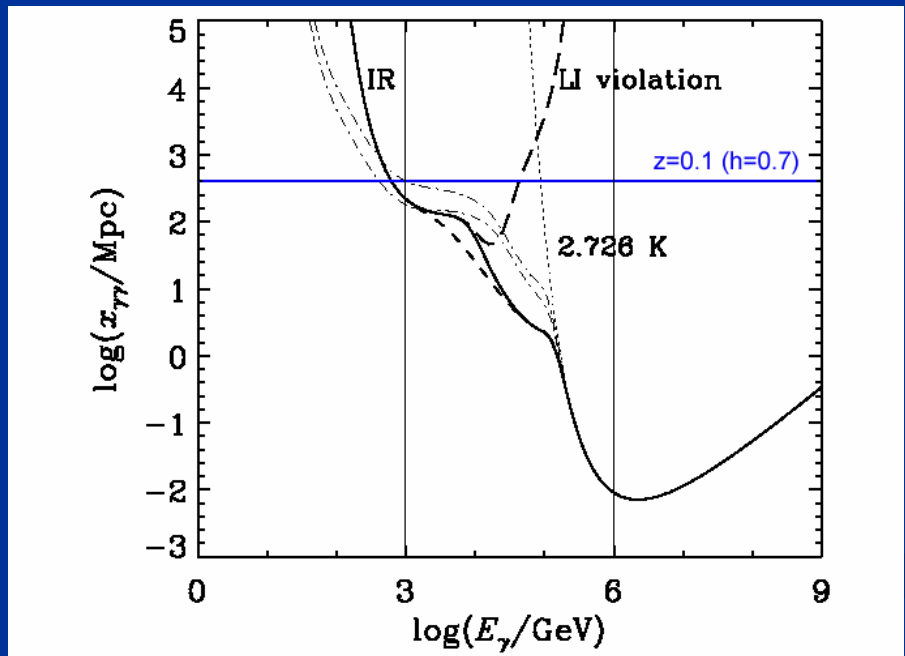
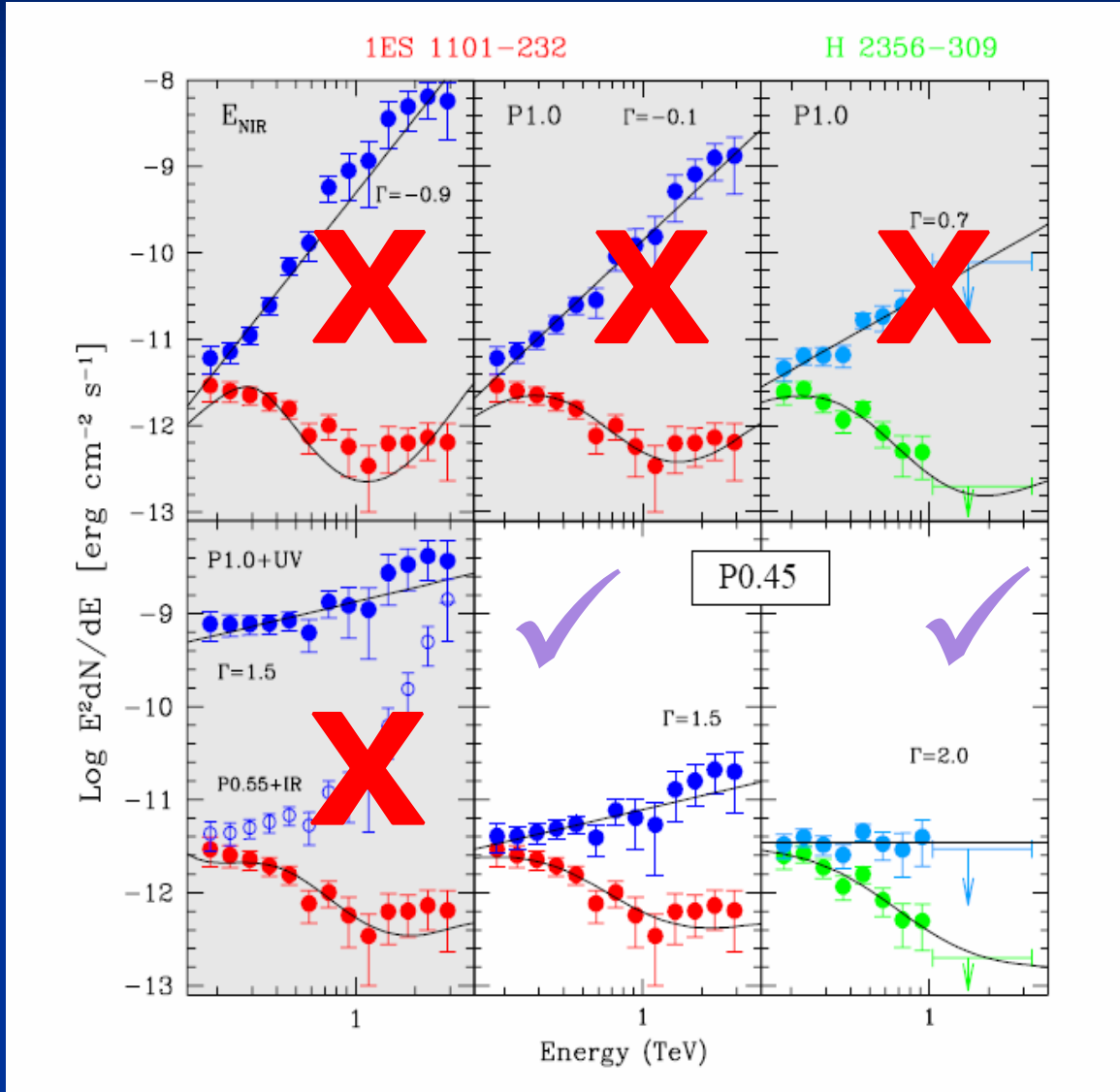
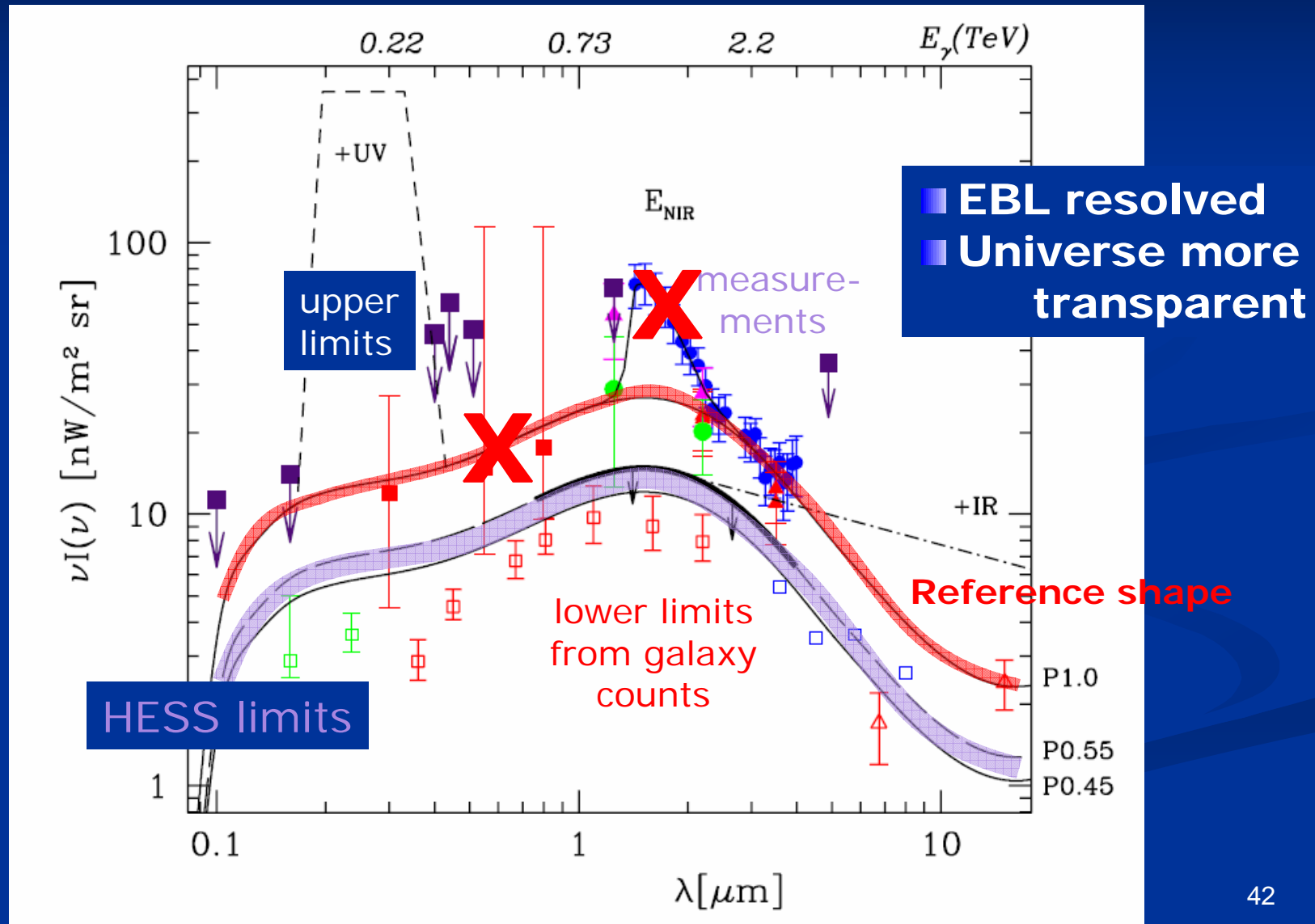


Figure 2: Mean free path for photon-photon pair production in the infrared-microwave background radiation. The curves correspond to those in Fig. 1 except that the effect of Lorentz Invariance violation discussed in Section 4 is shown by the long dashed curve.

# TeV gamma-ray absorption on EBL (2)



# EBL Spectra

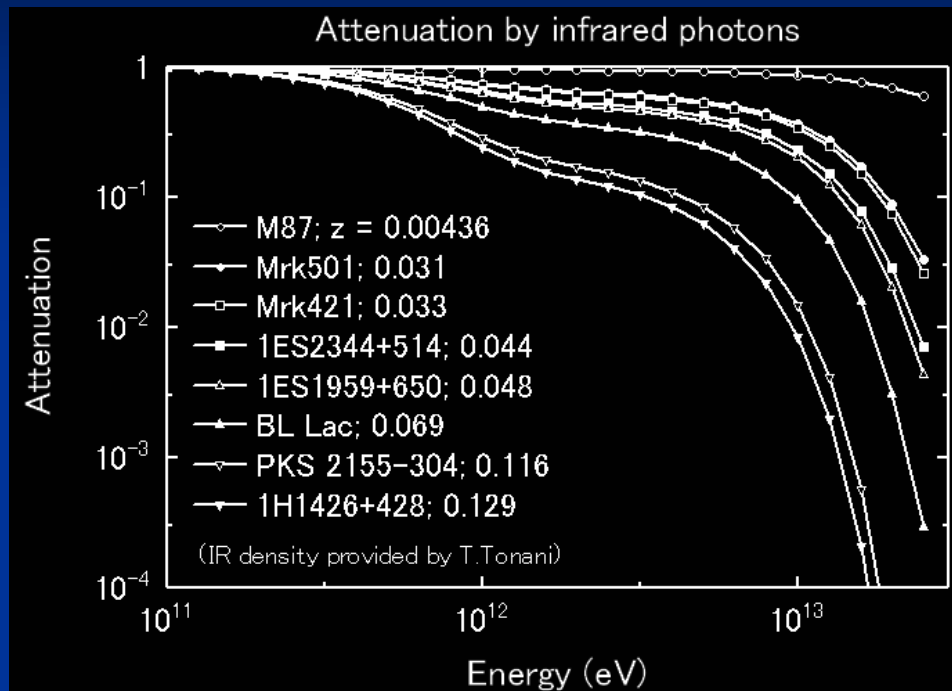


# AGN summary

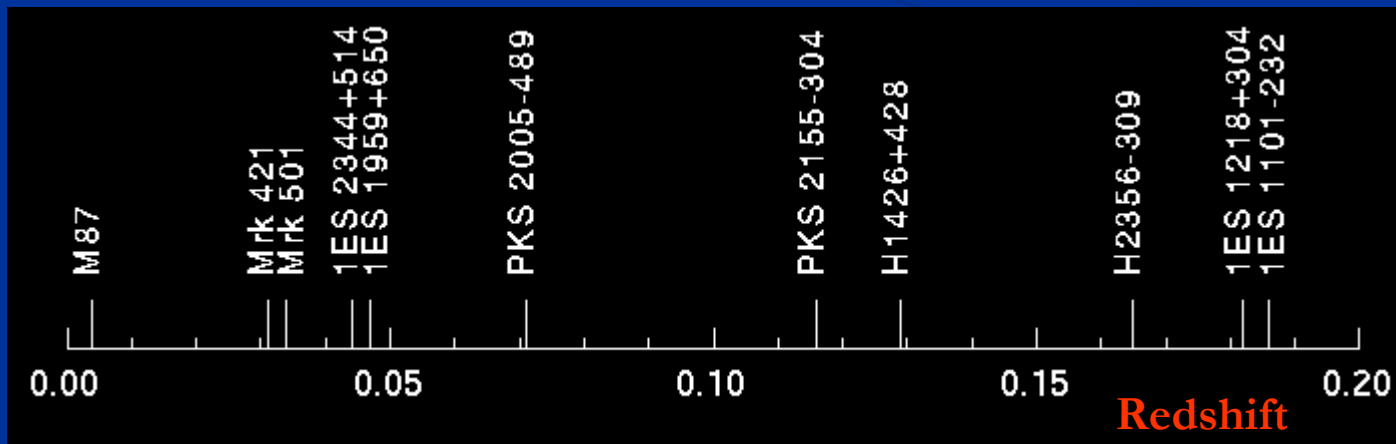
Source	Redshift	Type	First detection	Confirmation
M87	0.004	FR I	HEGRA	H.E.S.S.
Mrk 421	0.031	BL Lac	Whipple	Many
Mrk 501	0.034	BL Lac	Whipple	Many
1ES 2344+514	0.044	BL Lac	Whipple	HEGRA
1ES 1959+650	0.047	BL Lac	7TA	Many
<b>PKS 2005-489</b>	0.071	BL Lac	H.E.S.S.	
PKS 2155-304	0.116	BL Lac	Durham	H.E.S.S.
H1426+428	0.129	BL Lac	Whipple	Many
<b>H2356-309</b>	0.165	BL Lac	H.E.S.S.	
1ES 1218+304	0.182	BL Lac	MAGIC	
<b>1ES 1101-232</b>	0.186	BL Lac	H.E.S.S.	

⇒ Reaching further out in redshift!

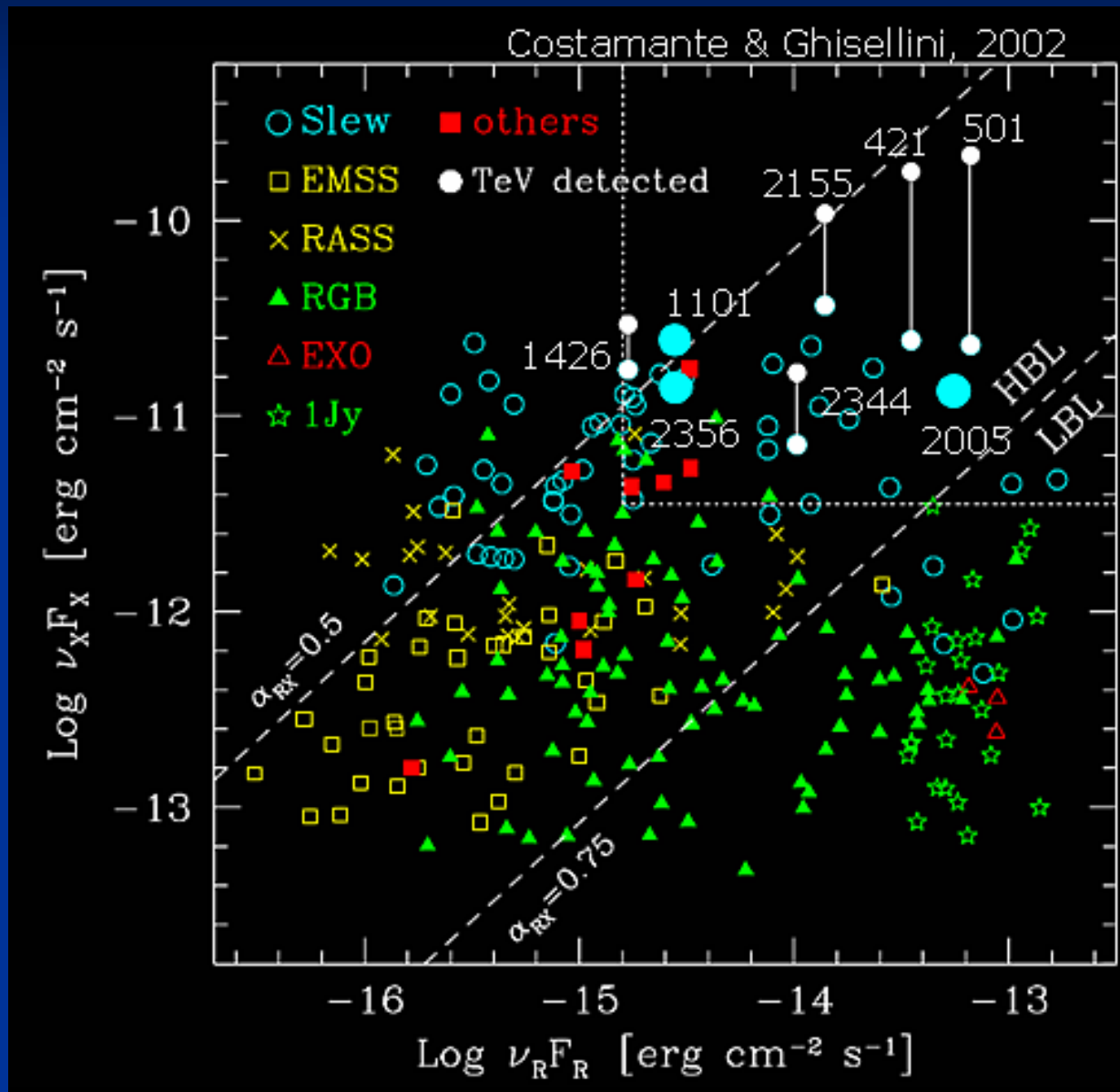
# TeV gamma-ray absorption on EBL (3)



We need many samples of AGNs at various redshifts!

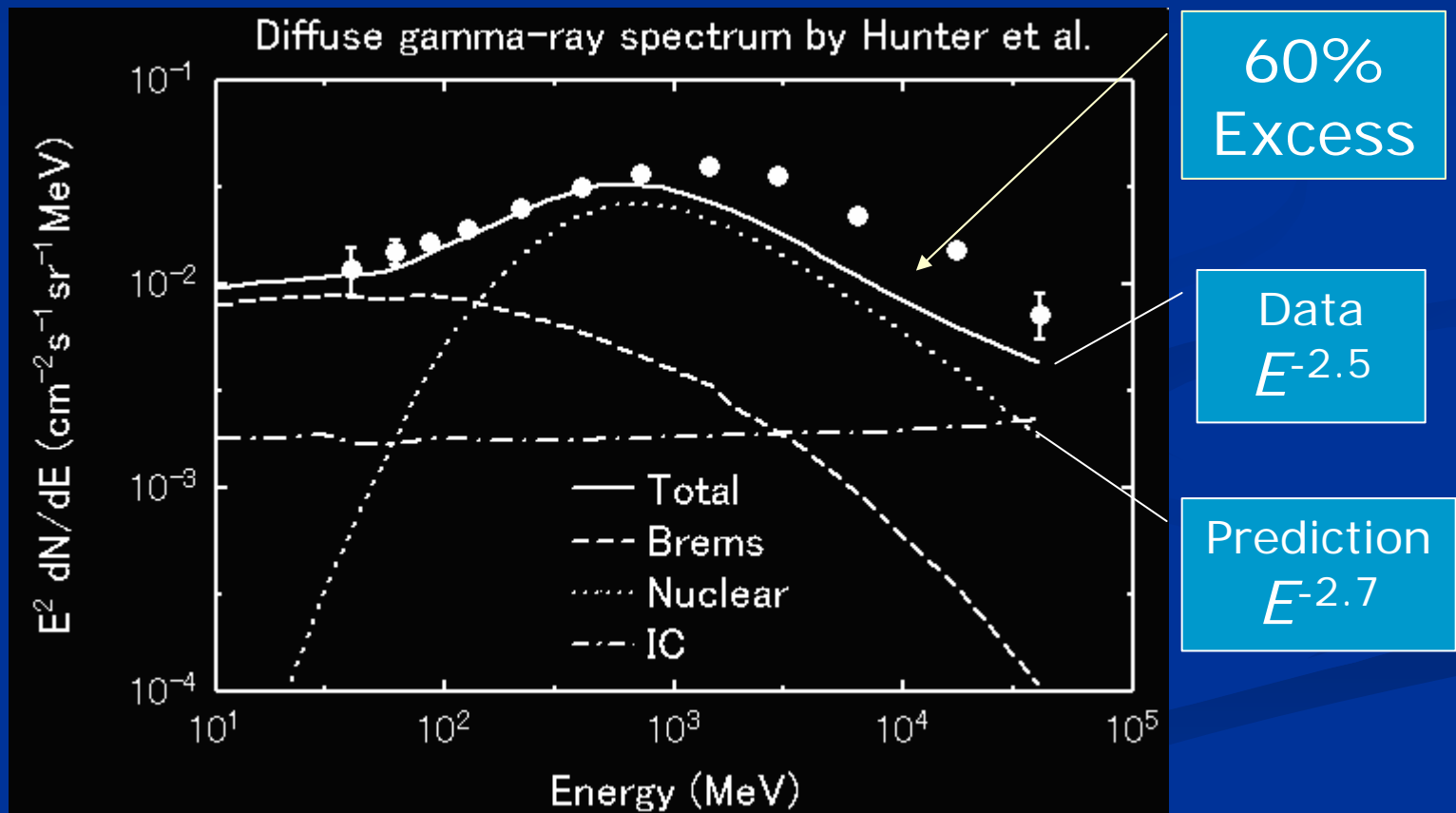


# TeV blazar population



# Galactic diffuse gamma-rays (1)

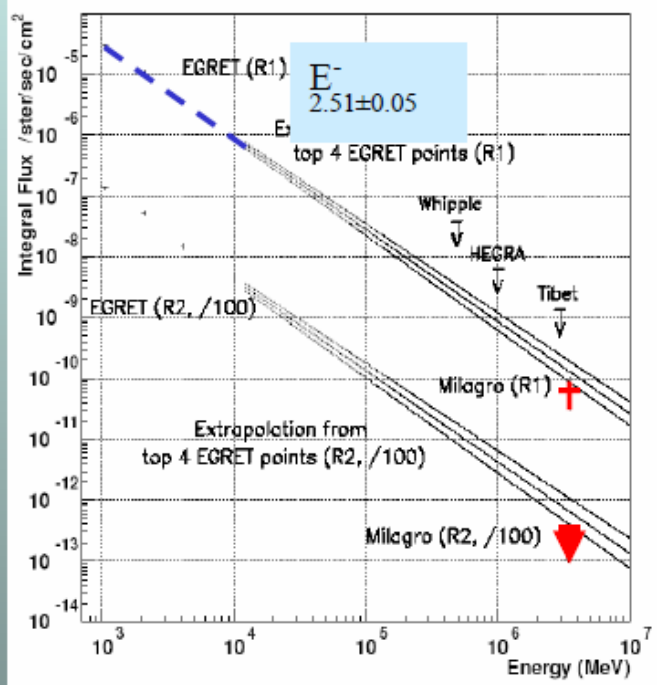
- EGRET “GeV bump” (Hunter et al. ApJ 1997)



# Galactic diffuse gamma-rays (2)

## OG 2.1: Diffuse $\gamma$ -ray Sources

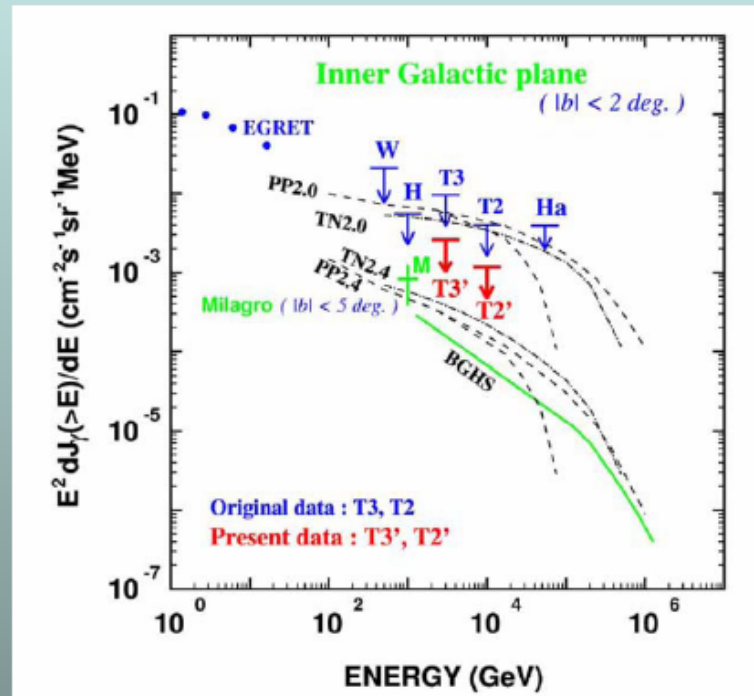
### 1. Galactic Plane



Milagro [Sinnis]

~  $4.5\sigma$  detection in 3 yr data set.  
Inner region:

$40\text{--}100^\circ$  in longitude,  $\pm 5^\circ$  in latitude

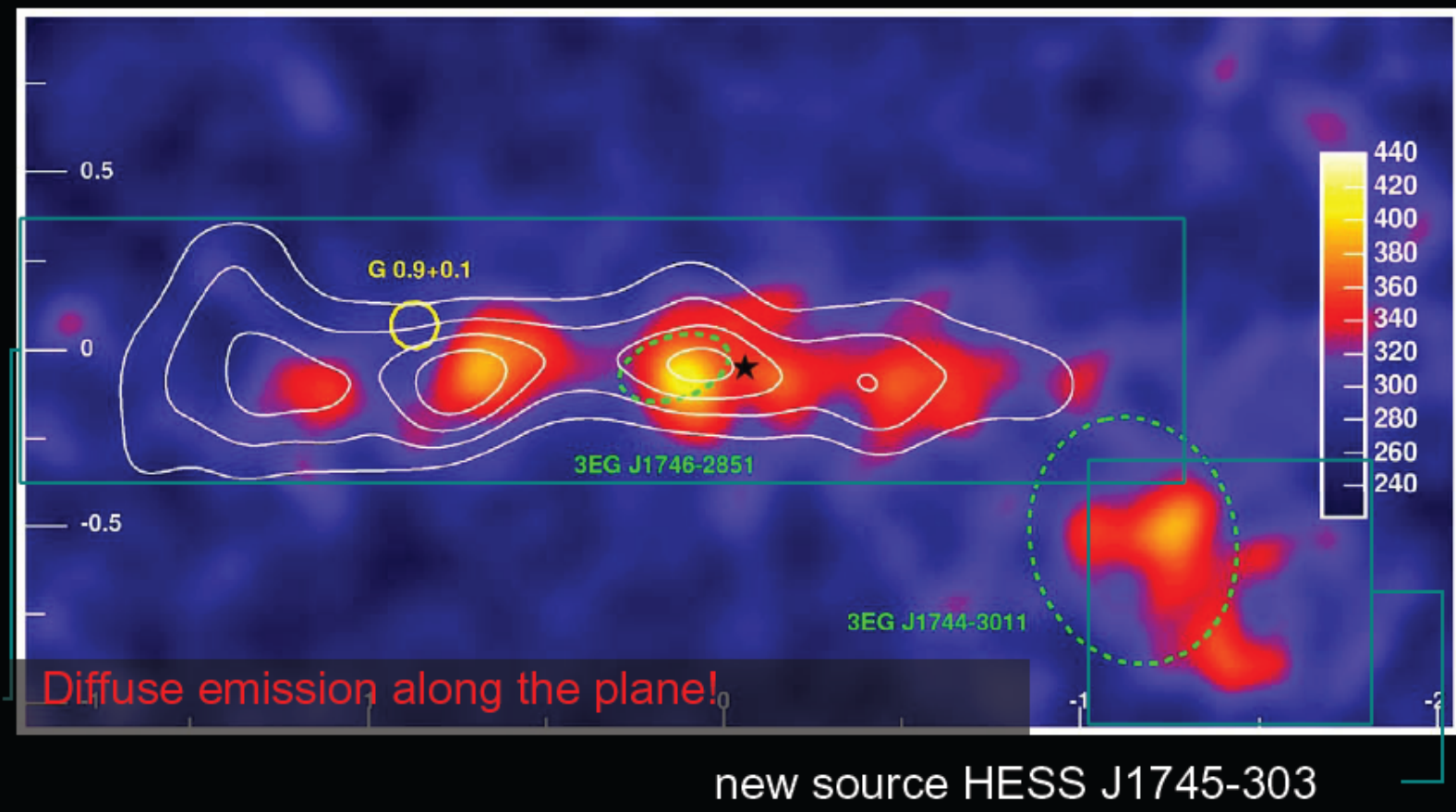


Tibet [Ohnishi]

Flux upper limit, consistent with  
Milagro detection.

# Diffuse gamma-rays along the plane?

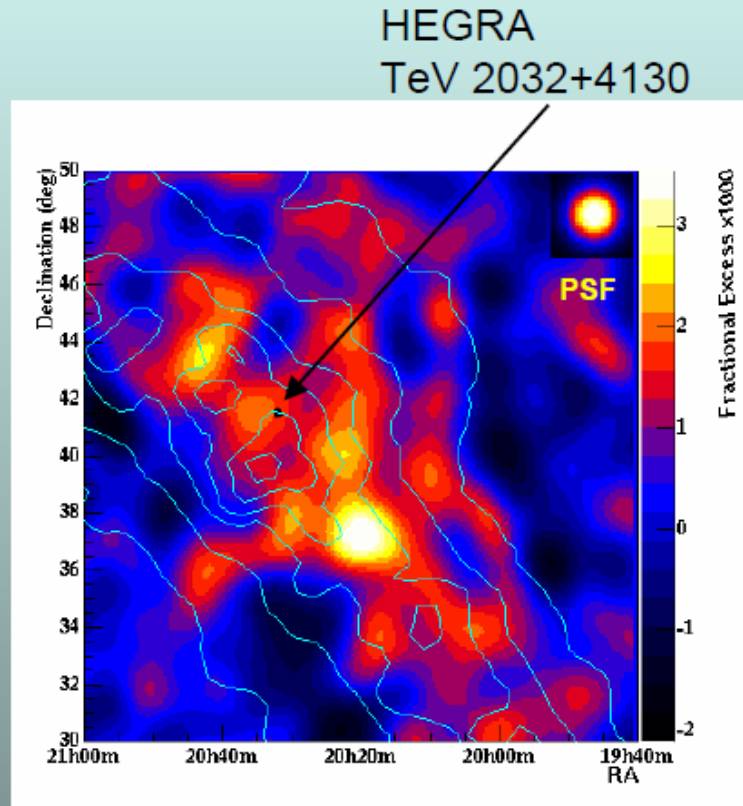
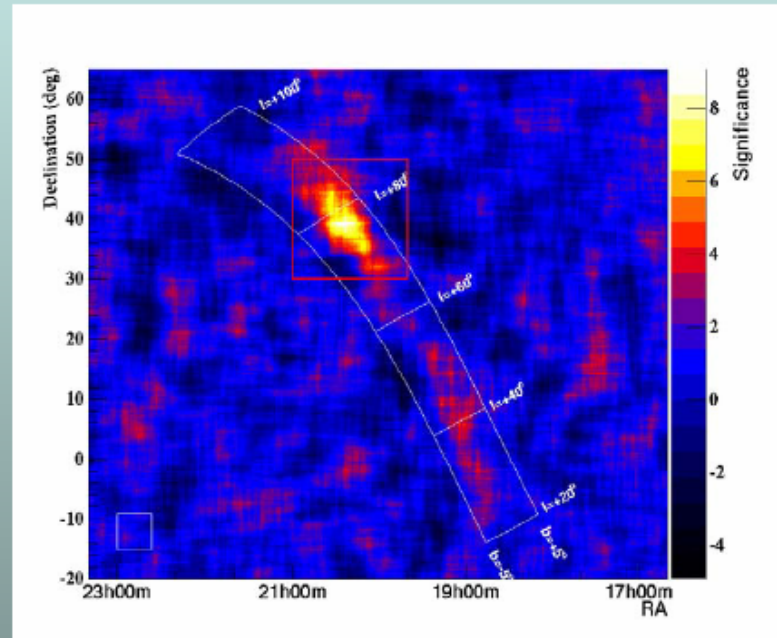
Residuals after source subtraction



# Diffuse source in Cygnus?

## OG 2.1: Diffuse $\gamma$ -ray Sources

### 2. Cygnus Region

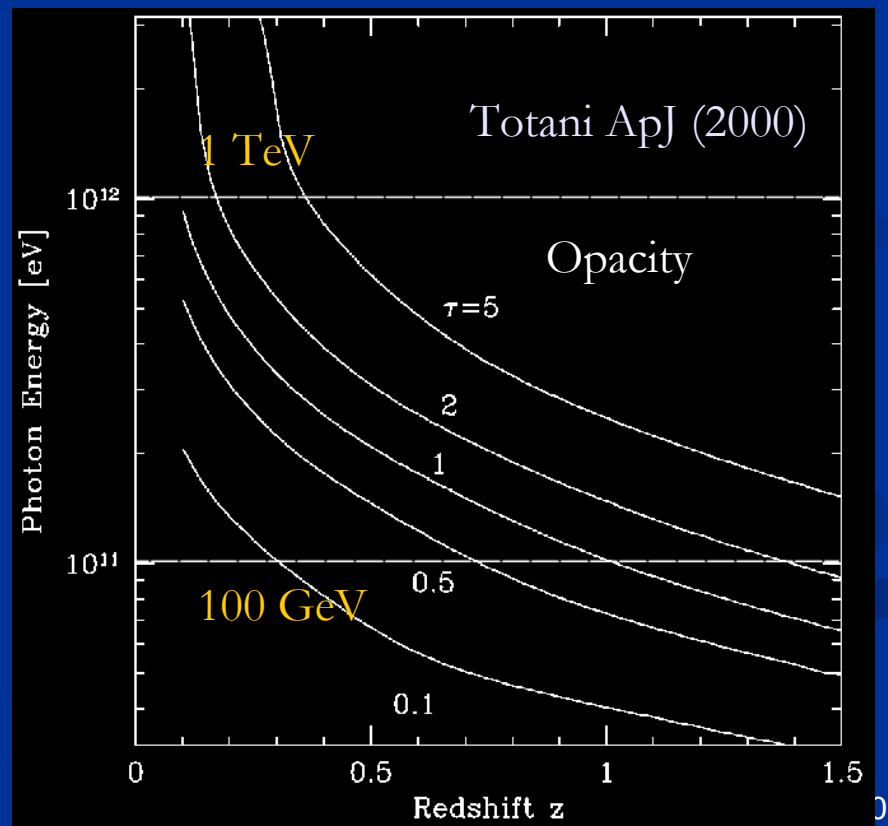


# Gamma Ray Bursts

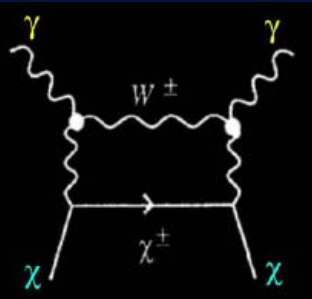
## ■ Ground-based experiments?

- TeV gamma-rays (afterglow)
  - MAGIC a few per year expected
- Air shower rate
  - Tibet-III
- Single particle rate
  - GRAND
  - ARGO-YBJ
  - Tibet-III

## ■ Need fast and precise GRB alerts!



# Dark matter annihilation

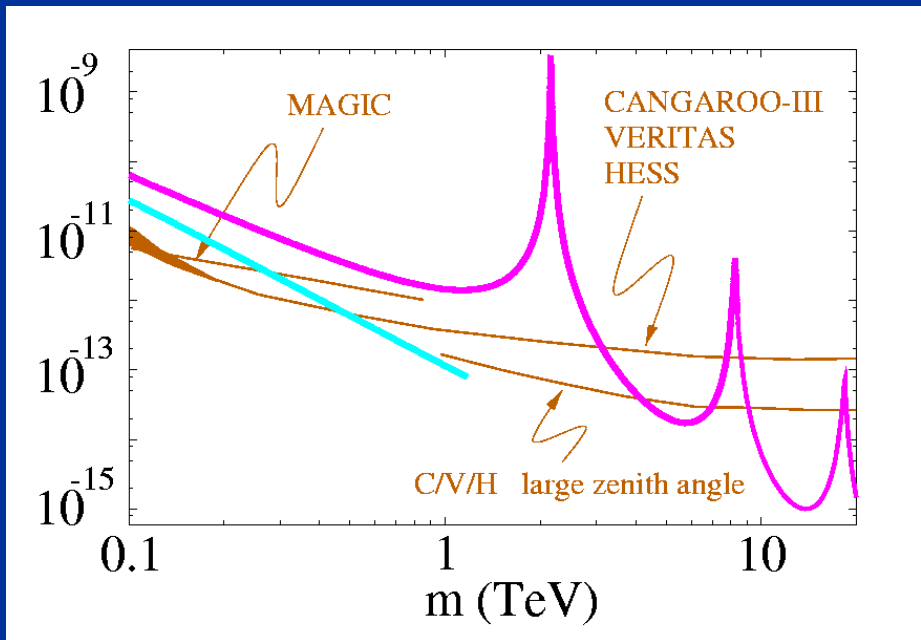


*Signal enhancement due to ‘cusp’ structure toward the center?*

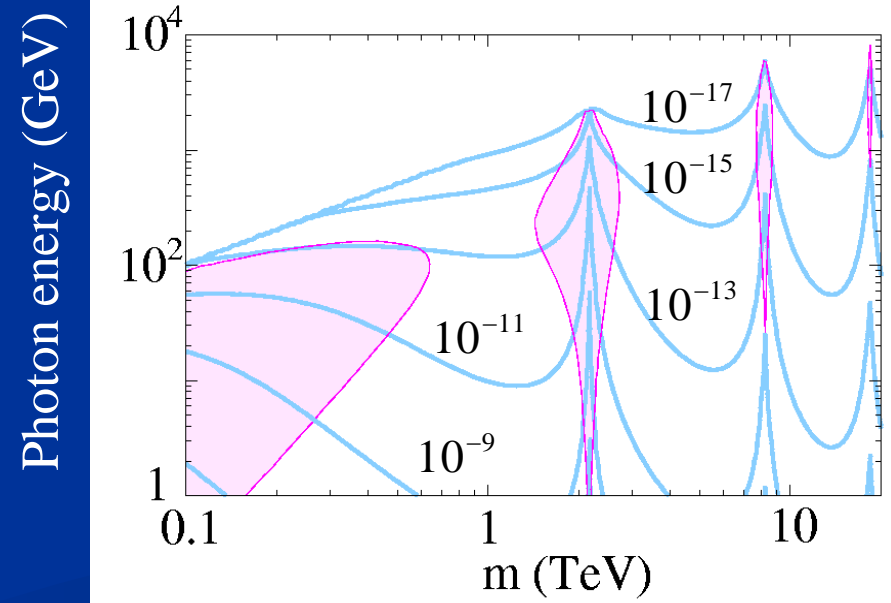
“*Explosive annihilation*” by non-perturbative effect

Line

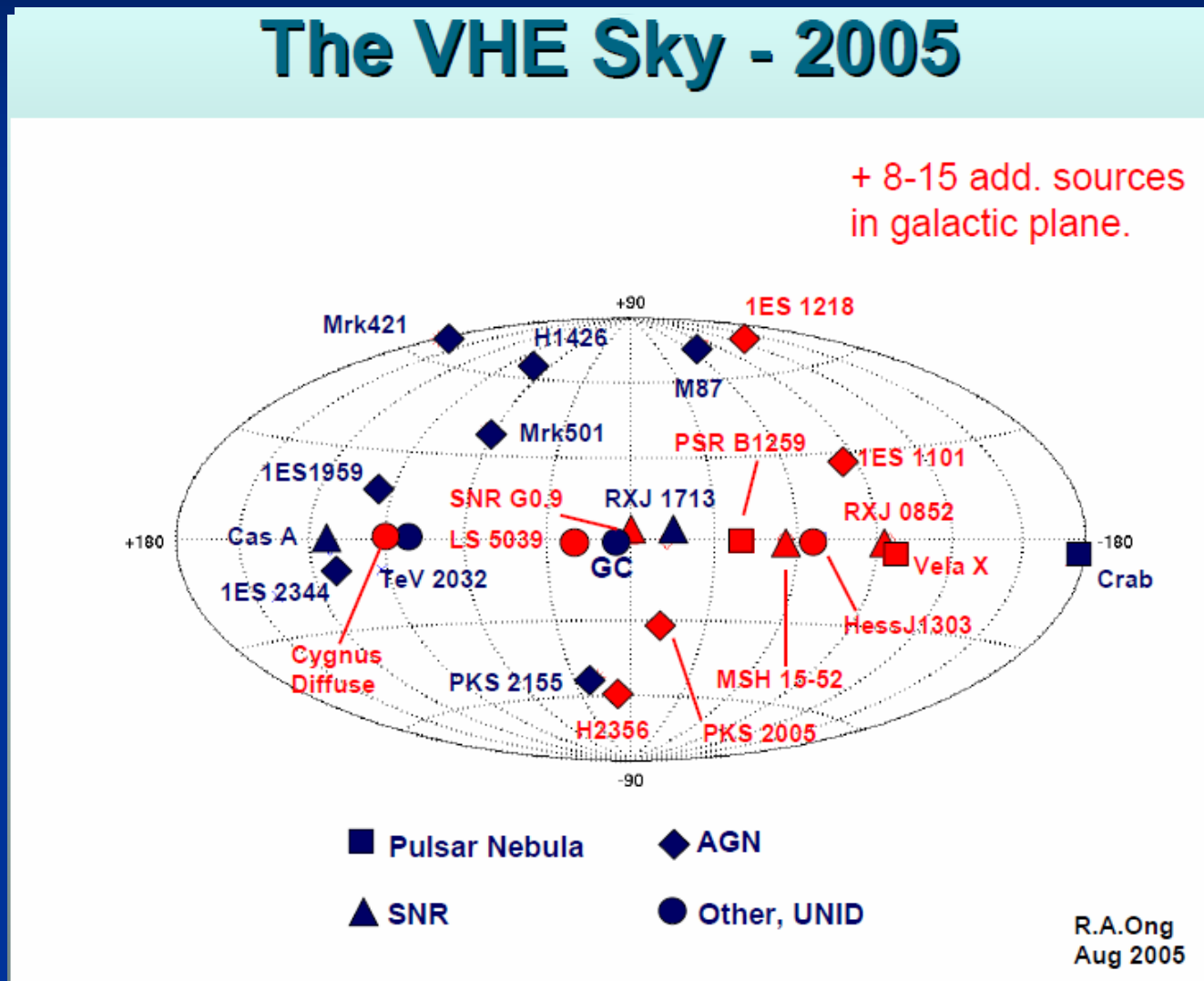
Flux ( $\text{cm}^{-2}\text{sec}^{-1}$ )    $\Delta\Omega = 10^{-3}$



Continuum

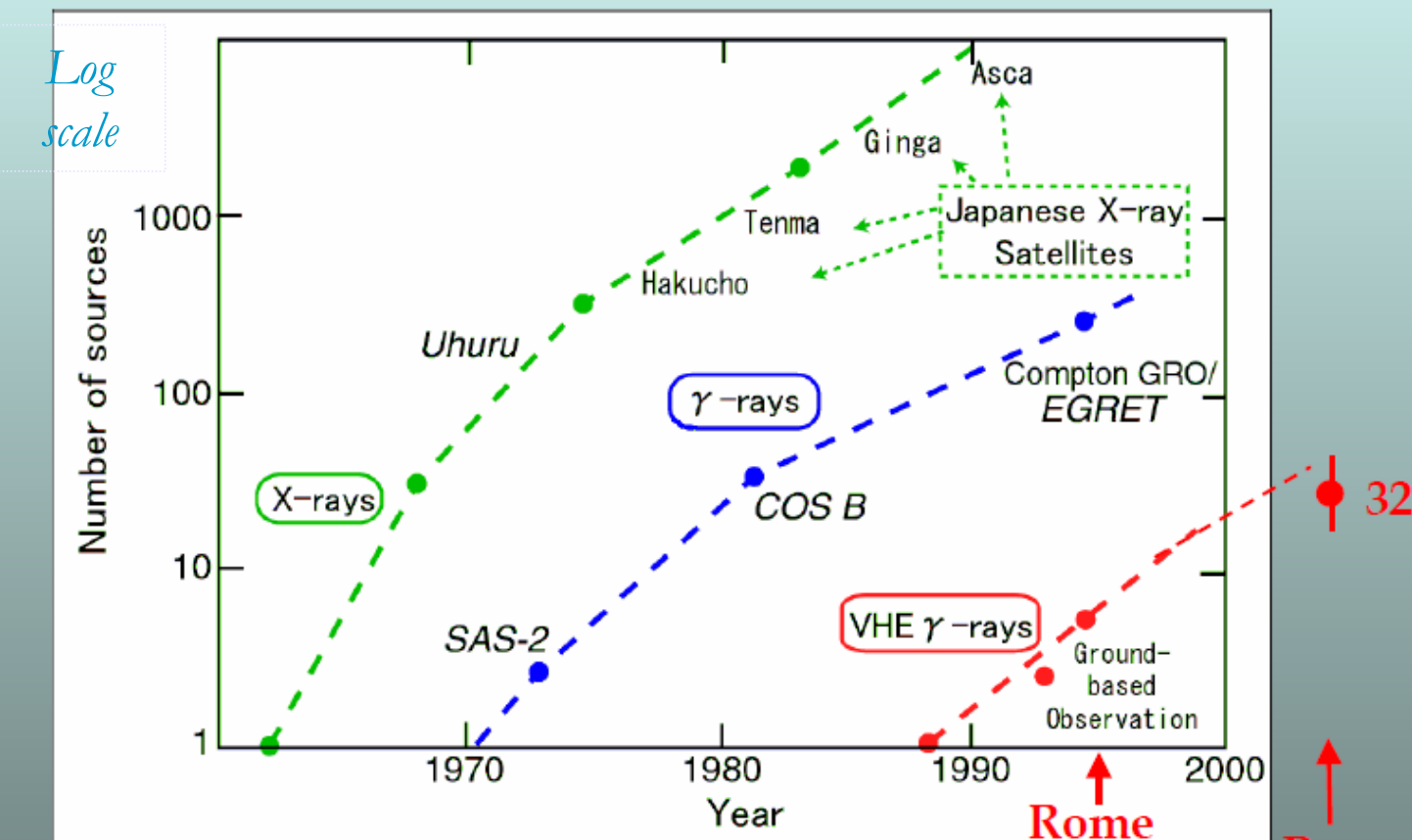


# “Evolution” of the TeV gamma-ray sky



# “Evolution” in number of objects

## “Kifune Plot”



Source count versus year  
[T. Kifune]

# VERITAS: VERITAS-4 by 2006



New site: Horseshoe canyon,  
Kitt Peak, Arizona

Smithsonian Inst. etc.

Prototype (Aug '03)

Nov 2005: New Environmental  
Assessment

Oct 2006: Completion of Phase I:  
4 telescope array

Then VERITAS-7 in 200X

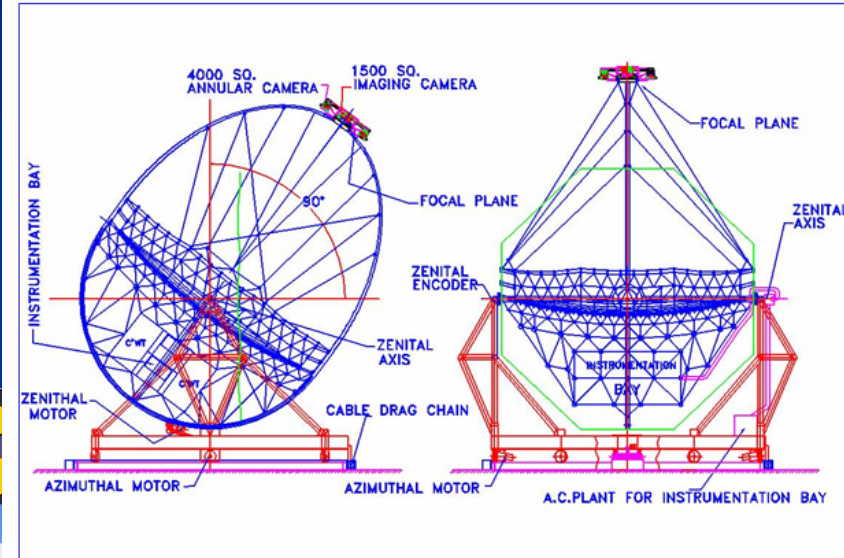


# Near future?

## THE NEXT STEP IN BOTH DIRECTIONS: HESS-II

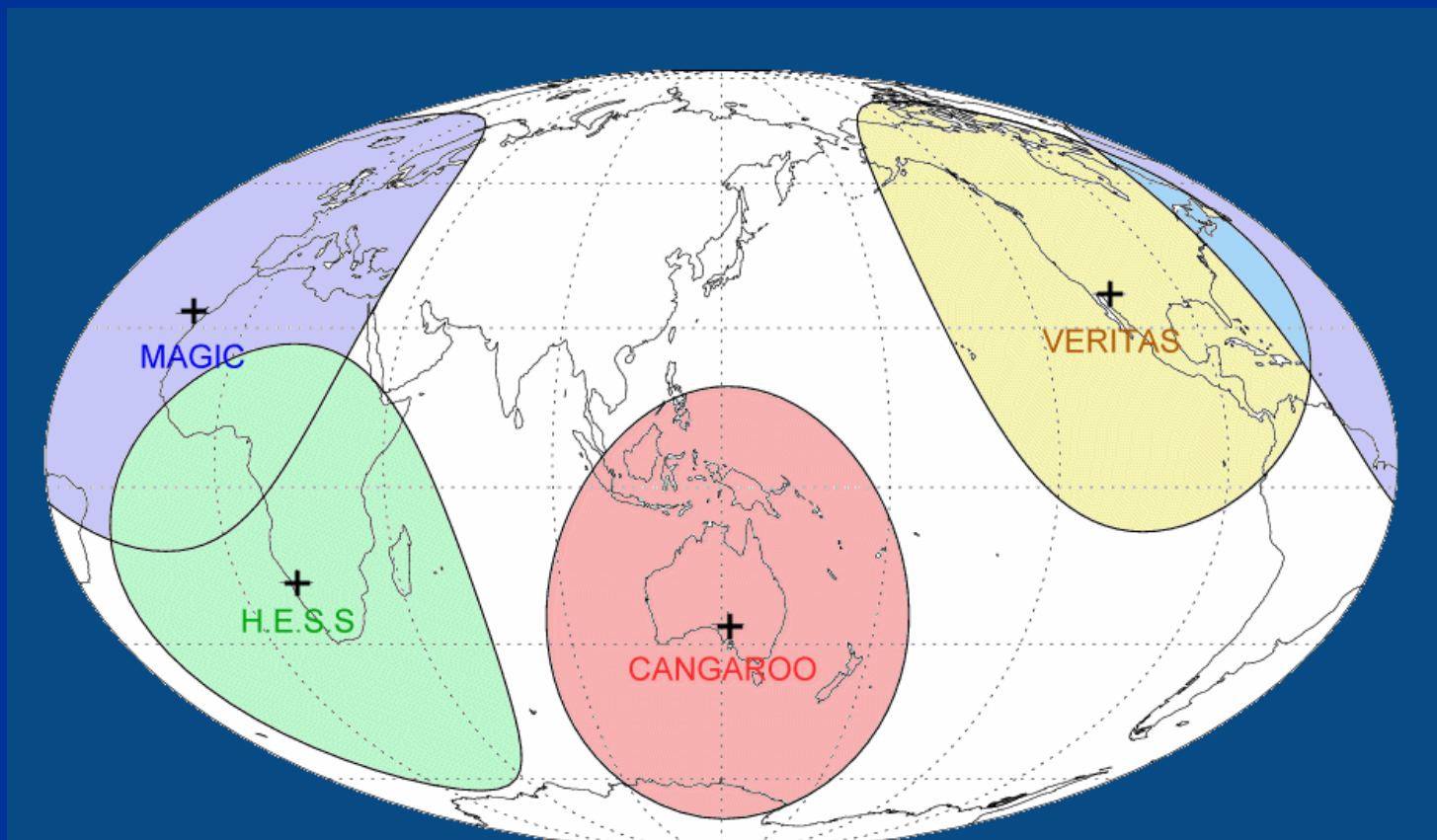


## MACE - 2 boom concept



# International coordination

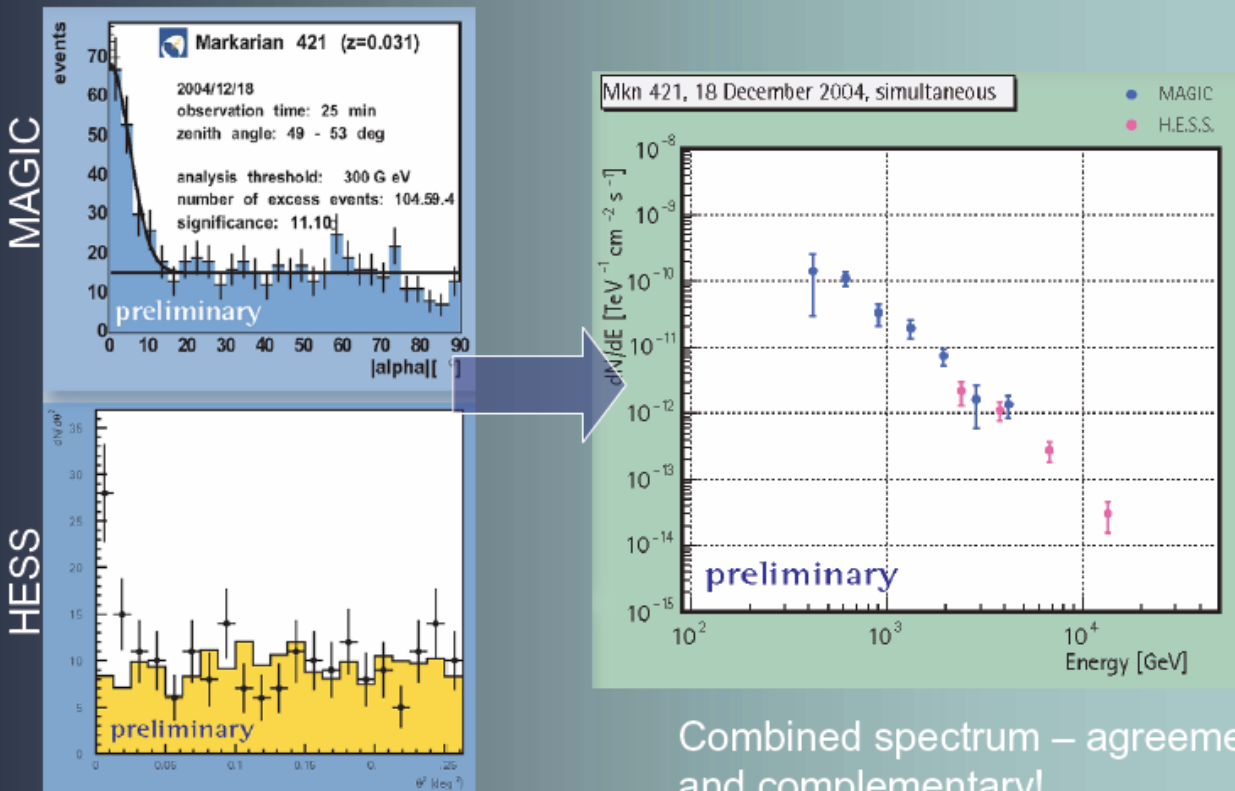
- Monitoring of time-variable objects (e.g. blazars)
- Multiwavelength observation campaign



# An example: MAGIC & H.E.S.S. campaign on Mrk 421

- Mrk 421 had the most active known period during 2004
- MAGIC has observed this object for ~14 hours in different emission states (total significance of the detection is above  $40\sigma$ )
- MAGIC and HESS first combined observation of AGN Mrk421 during December 2004

Mrk421



Combined spectrum – agreement  
and complementary!

# Summary

- Very high energy sources may contain large varieties, including both galactic and extragalactic objects.
- Supernova remnants are confirmed to be very-high-energy particle accelerators: an important evidence of cosmic ray origin!
- TeV gamma-ray astronomy is becoming an indispensable field of astronomy.
- The “third generation” Cherenkov telescopes are working hard (and “fourth” ones are planned)— more fun!